

Key Points:

- U-Pb zircon dating and geological mapping confirm a folded thrust-stack along part of the southern margin of the Archean Barberton Greenstone Belt (BGB)
- Forward modeling of a balanced cross-section indicates >33 km of horizontal shortening toward the northwest
- Vertically- and horizontally-dominated tectonics interfered with each other in the BGB and may have done so in other Archean greenstone belts as well

Supporting Information:

Supporting Information may be found in the online version of this article.

Correspondence to:

C. Heubeck,
christoph.heubeck@uni-jena.de

Citation:

Heubeck, C., Thomsen, T. B., Heredia, B. D., Zeh, A., & Balling, P. (2023). The Malolotsha Klippe: Large-scale subhorizontal tectonics along the southern margin of the Archean Barberton Greenstone Belt, Eswatini. *Tectonics*, 42, e2022TC007359. <https://doi.org/10.1029/2022TC007359>

Received 20 APR 2022
Accepted 3 NOV 2022

Author Contributions:

Conceptualization: Christoph Heubeck
Data curation: Christoph Heubeck, Tonny B. Thomsen, Armin Zeh
Formal analysis: Armin Zeh, Philipp Balling
Funding acquisition: Christoph Heubeck
Investigation: Christoph Heubeck, Tonny B. Thomsen, Benjamin D. Heredia, Philipp Balling
Methodology: Tonny B. Thomsen, Armin Zeh

© 2022. The Authors.

This is an open access article under the terms of the [Creative Commons Attribution-NonCommercial-NoDerivs License](#), which permits use and distribution in any medium, provided the original work is properly cited, the use is non-commercial and no modifications or adaptations are made.

The Malolotsha Klippe: Large-Scale Subhorizontal Tectonics Along the Southern Margin of the Archean Barberton Greenstone Belt, Eswatini

Christoph Heubeck¹ , Tonny B. Thomsen², Benjamin D. Heredia² , Armin Zeh³, and Philipp Balling¹

¹Department of Geosciences, Friedrich-Schiller Universität Jena, Jena, Germany, ²The Geological Survey of Denmark and Greenland (GEUS), Copenhagen, Denmark, ³KIT - Karlsruher Institut für Technologie, Campus Süd, Institut für Angewandte Geowissenschaften, Mineralogie und Petrologie, Karlsruhe, Germany

Abstract Whether Archean tectonics were horizontally or vertically dominated is controversially discussed because arguments bear on the kinematics and thermal state of the Archean mantle and constrain the mode of formation of the earliest continental crust. Highly deformed strata of Archean greenstone belts figure prominently in this debate because they record long periods of time and multiple deformation phases. Among the best-preserved greenstone belts counts the Barberton Greenstone Belt (BGB) of southern Africa. Geological mapping of part of the southern BGB in Eswatini (Swaziland), combined with U-Pb zircon dating, shows that the region preserves a tightly re-folded imbricate thrust stack in which metavolcanic and -volcaniclastic strata of the Onverwacht Group, deposited at 3.34–3.29 Ga, have been thrust on top of ca. 3.22 Ga siliciclastic strata of the Moodies Group. The structurally highest element, the Malolotsha Syncline, forms a tectonic klippe of substantial size and is >1,450 m thick. Forward modeling of a balanced cross section indicates that this thrust stack was part of a northwestward-verging orogen along the southern margin of the BGB and records a minimum horizontal displacement of 33 km perpendicular to its present-day faulted, ductily strained and multiply metamorphosed margin. Because conglomerate clasts indicate a significantly higher degree of prolate strain which extends further into the BGB than at its northern margin, late-stage tectonic architecture of the BGB may be highly asymmetrical. Our study documents that the BGB, and perhaps other Archean greenstone belts, preserves a complex array of both vertically- and horizontally-dominated deformation styles that have interfered with each other at small regional and short temporal scales.

Plain Language Summary Worldwide, only a few regions exist where ancient rock strata document how earth cooled, surface strata deformed, and continents grew. It is debated whether vertical movements dominated (akin to a lava lamp) and when major horizontal motions (as they dominate Earth today) began; certainly, there was also overlap between these regimes. Radiometric age dating of zircons extracted from strata along the southern margin of one of the best-preserved ancient regions in southern Africa, the Barberton Greenstone Belt in Eswatini, show that older strata were thrust there over younger strata for at least 33 km distance subhorizontally. Then they were shingled, and then folded. The results show that even at a time when Earth's oldest continents were just forming, significant horizontal displacements existed already.

1. Introduction

Although the history of early Archean continental crust has long been simplistically interpreted as either having been dominated by vertical or by subhorizontal tectonics, many recent models recognize that both modes may have overlapped in time and space (Bédard, 2006, 2018; Cawood et al., 2006; Condie & Kröner, 2008; Palin et al., 2020; Van Kranendonk, 2011b), thus suggesting a drawn-out transition from a largely nonactualistic mode of large-scale surface deformation to the present-day plate-tectonic modus operandi.

Because of its considerable size, good exposure, variable lithologies covering ca. 350 Myr of Earth history, and its low degree of metamorphic overprint, the Barberton Greenstone Belt (BGB) in the basement of the Kaapvaal Craton has received significant attention and been at times at the center of contention (e.g., de Ronde & de Wit, 1994; de Wit et al., 1983, 1992, 2018; Kröner & Hofmann, 2019; Lowe & Byerly, 2007). Geochemical, structural, and stratigraphic studies have increasingly shown that the BGB is not a first-order symmetrical, sagged synformal structure (Anhaeusser, 1984; Anhaeusser et al., 1968) but asymmetrical in terms of style of deformation, the history of adjacent magmatic terranes, and basin structure (Byerly et al., 2019; Diener

Project Administration: Christoph Heubeck
Resources: Christoph Heubeck, Tonny B. Thomsen, Armin Zeh
Software: Tonny B. Thomsen, Benjamin D. Heredia, Armin Zeh, Philipp Balling
Validation: Christoph Heubeck, Benjamin D. Heredia, Armin Zeh, Philipp Balling
Visualization: Christoph Heubeck, Tonny B. Thomsen, Benjamin D. Heredia, Philipp Balling
Writing – original draft: Christoph Heubeck
Writing – review & editing: Christoph Heubeck, Tonny B. Thomsen

et al., 2005, 2006; Dziggel et al., 2005; Kisters et al., 2003, 2010; Lowe & Byerly, 1999; Moyen et al., 2018; Schmitz & Heubeck, 2021). Recent studies (Cutts et al., 2014; Kröner et al., 2018; Lana et al., 2011) have highlighted fundamental differences in the history of rocks to the north(west) and south(east) of the BGB, gradually relating the high-temperature deformation history seen in the high-grade polymetamorphic rocks of the Ancient Gneiss Complex (AGC; Jackson & Robertson, 1983; Jackson, 1984; Kröner et al., 1989, 1991, 1996; Kröner & Tegtmeyer, 1994; Zeh et al., 2011) in the south to the brittle-ductile pattern of folding and faulting within the BGB supracrustal sequence. We here contribute new structural, stratigraphic and geochronologic data from the southern margin of the BGB, thereby strengthening and extending an earlier finding (Lamb, 1984; Lamb & Paris, 1988) of large-scale subhorizontal transport perpendicular to this margin.

2. Regional Geology and Problem Statement

The Malolotsha (or Malolotja) Syncline, located in Eswatini, is a large synclinal structure in the southern BGB near its margin to younger plutonic rocks. It is ca. 11 × 6 km in size and lies almost entirely within the grasslands of the Malolotsha Nature Reserve (Figures 1 and 2; Urie, 1970, 1971; Barton, 1982; Lamb, 1984; Lamb & Paris, 1988). The core of the syncline consists of foliated talc schists, likely representing regionally altered and penetratively deformed (ultra-)mafic volcanic rocks, interbedded with a few isolated chert beds. The synclinal core is surrounded on its eastern and western limb and in the exposed up-plunge hinge zone by km-thick, thick-bedded, uniformly stratigraphically upward- and inward-facing quartzose metasandstones with rare, bedding-parallel interleaved strips of poorly exposed talc schists. The contact between the quartzose sandstones and the overlying talc schists in the core of the syncline is bedding-plane parallel. It represents a plane of very high competence contrast and is therefore always sheared in the few places where it is exposed (Figures 3c and 3e). The syncline is tight and plunges gently (ca. 18°) south where it is covered by Quaternary sediments.

The Fe- and Mg-rich composition of the talc schists and its >1 km thickness suggest a correlation with komatiitic and basaltic protoliths of the ca. 8–10 km thick Onverwacht Group of the BGB formed at ca. 3,560,3280 Ma (Byerly et al., 1996, 2019; Lamb, 1984). In the southern BGB, strata of the Onverwacht Group are overlain by strata of the Diepgezet Group (Lamb, 1987; Lamb & Paris, 1988; “Group B” of Lamb, 1984), which is, at least lithostratigraphically, correlative with the Fig Tree Group of South Africa. Overlying quartzose sandstones, estimated to be at least 1.8 km thick and informally named “Group A” by Lamb (1984) and “Malolotsha Group” by Lamb (1987) and Lamb and Paris (1988), are identical or similar in lithology, sedimentary facies, petrographic composition, age, and thickness to strata of the Moodies Group of the BGB, ca. 3,223–3,215 Ma old (Heubeck, 2019; Heubeck et al., 2013; Heubeck, Drabon, et al., 2022; Heubeck, Thomsen, et al., 2022; Zeh et al., 2013) to which they can be correlated along strike across the South African-Eswatini border (Anhaeusser et al., 1983; Lamb, 1986; Visser et al., 1956). Because neither the Diepgezet Group nor the Malolotsha Group are formally registered in the stratigraphic nomenclature of southern Africa, and because both have clear equivalents in earlier defined and better-studied units in South Africa (Fig Tree and Moodies Groups, respectively) into which they trend obliquely across the international border, we will therefore in the following use the latter two names.

Moodies Group strata constitute the youngest unit of the BGB and have, with the sole exception of the Malolotsha region, nowhere an upper contact (Figures 1 and 2). Lamb (1984) recognized the unusual stratigraphic superposition of likely Onverwacht-age metavolcanics over the Moodies Group (meta)-siliciclastics and interpreted the Malolotsha Syncline core as a synformally folded tectonic klippe in which older, Onverwacht-age strata were thrust over a lithotectonic complex of younger Moodies-age-equivalent strata along a low-angle thrust. Lamb (1984, 1986) estimated a horizontal translation of at least 10 km, which is an interpretation that we here support, modify, and expand by zircon U-Pb dating and structural analysis.

3. Methods

We mapped the geology of the Malolotsha Syncline at a scale of approximately 1:5,000 intermittently, mostly during the winter months 2017–2021, with an emphasis on mappable structural deformation and lithology. We sampled lithologies of the Moodies Group (conglomerates, sandstones, minor shales) for thin-section petrography, measured orientation and dimensions of in-situ conglomerate clasts for strain analysis, and sampled the silicified volcanic and volcanoclastic strata (“cherts”) interbedded with the talc schists for petrography and zircon

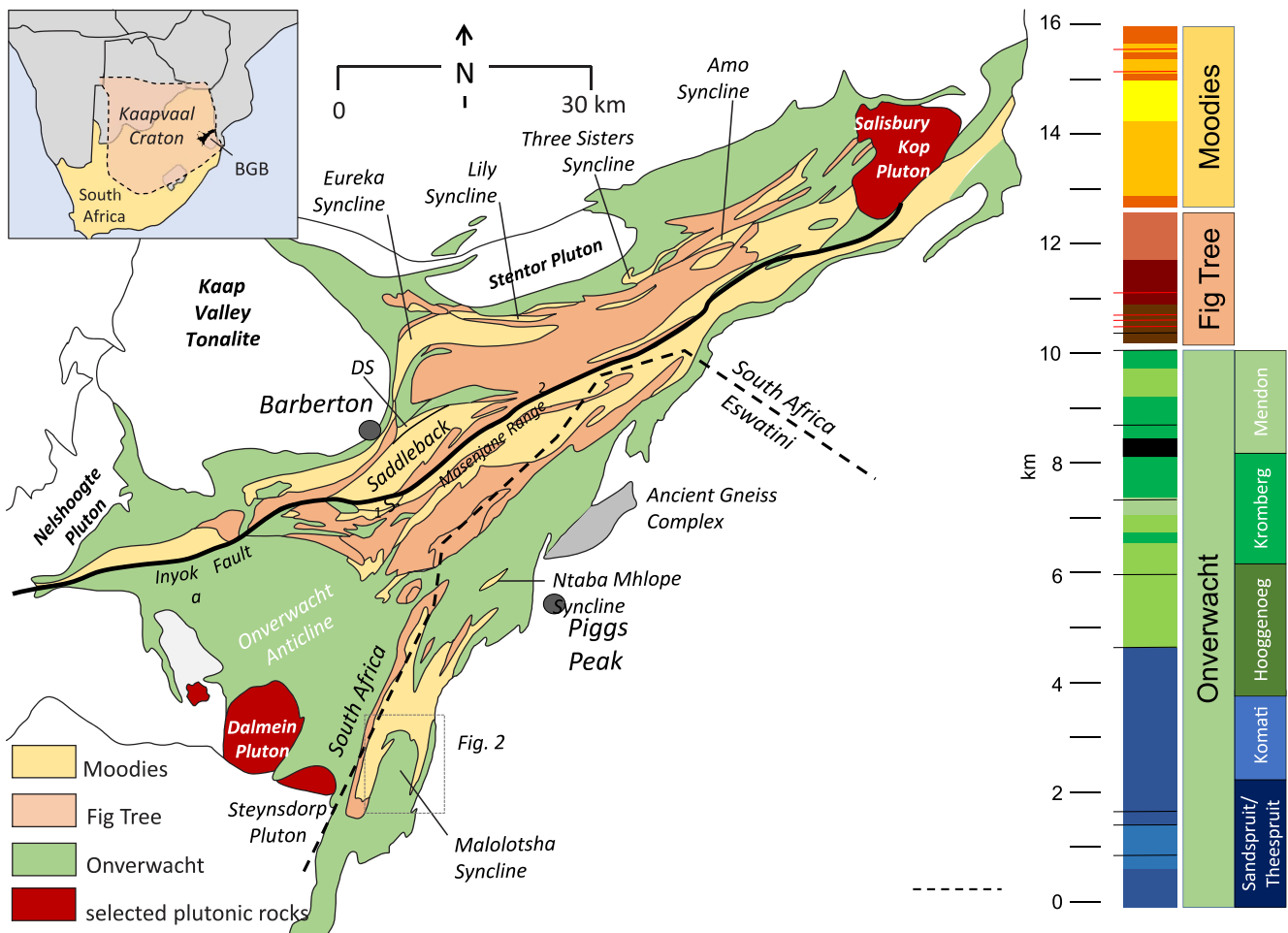


Figure 1. Simplified geological map of the Barberton Greenstone Belt (BGB), emphasizing (litho-)stratigraphic units. Inset map shows location of the BGB in southern Africa. The Malolotsha Syncline (boxed) forms a large south-plunging syncline in the far southern BGB in Eswatini.

U-Pb dating. Raman spectroscopy aided in the identification of metamorphic index minerals and opaque heavy minerals.

Rock processing for the U-Pb zircon dating followed a routine workflow of crushing, milling, sieving, heavy liquid separation, magnetic separation, and hand picking of zircon grains. Four of the six samples collected yielded a sufficient number of zircon grains for the dating. Sample 18–270 was dated at the Goethe University Frankfurt (GUF) am Main, Germany, whereas samples 19–122, 19–130, and 19–133 were dated at the Geological Survey of Denmark and Greenland (GEUS), Copenhagen.

U-Pb dating was carried out on mineral grain separates embedded in epoxy mounts by laser ablation inductively coupled plasma mass spectrometry. At the GUF, U, Th and Pb isotopes of the zircon grains were analyzed using a Thermo Fisher Scientific Element 2 sector field ICP-MS coupled to a Resolution M-50 (Resonetics) 193 nm ArF excimer laser ablation system (ComPexPro 102F, Coherent) equipped with a two-volume ablation cell (Laurin Technic, Australia). Data were acquired in time resolved—peak jumping—pulse counting/analog mode over 466 mass scans, with a 20 s background measurement followed by 21 s sample ablation. Laser spot-size was 33 μm for unknowns and the standard zircons GJ-1 (primary standard), BB and Plešovice (secondary standards). The sample surface was cleaned directly before each analysis by three pulses pre-ablation. Ablations were performed in a 0.6 l min^{-1} He stream, which was mixed directly after the ablation cell with 0.007 l min^{-1} N_2 and 0.83 l min^{-1} Ar prior to introduction into the Ar plasma of the SF-ICP-MS. All gases had a purity of >99.999% and no homogenizer was used for mixing the gases to prevent smoothing of the signal. Signal was tuned for maximum sensitivity for Pb and U while keeping oxide production, monitored as $^{254}\text{UO}/^{238}\text{U}$, below 0.3%. The

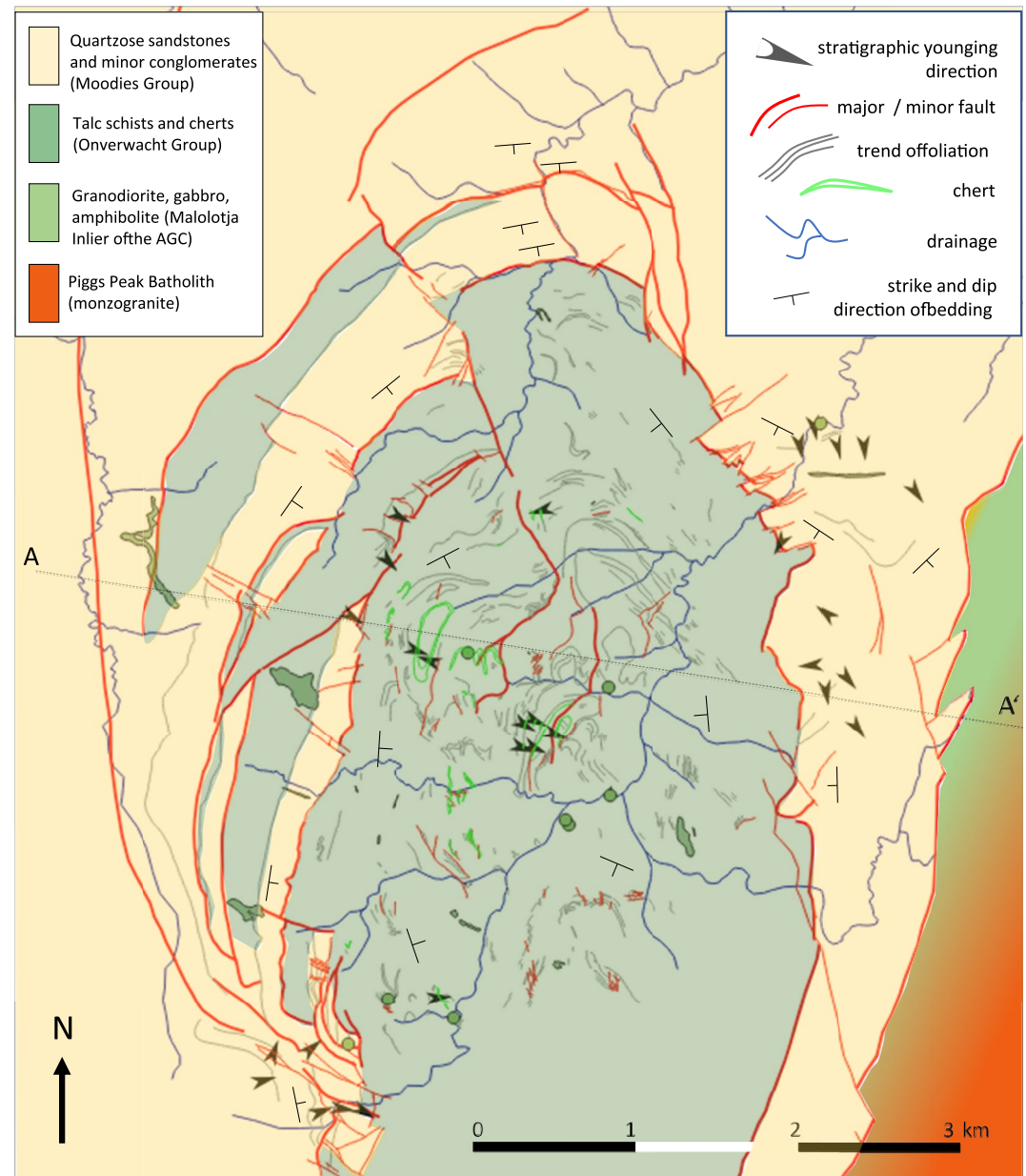


Figure 2. Simplified geological map of the Malolotsha Syncline area (Geological Survey of Swaziland, 1970; Lamb, 1984; own mapping). Talc schists and thin cherts in the center of the syncline are ca. 3,340–3,310 Ma in age. They correlate in age and lithology with Onverwacht strata (upper Kromberg and lower Mendon Formations; see Figure 1). Moodies strata surrounding the synclinal core are ca. 3,223–3,210 Ma old and face inwards; the contact is nowhere exposed.

sensitivity achieved was in the range of 12,000–17,000 cps/ $\mu\text{g g}^{-1}$ for ^{238}U with a 33 μm spot size, at 5.5 Hz and 5 J cm^{-2} laser energy, at a RF power of 1235 W. Raw data were corrected offline for background signal, common Pb, laser induced elemental fractionation, instrumental mass discrimination, and time-dependent elemental fractionation of Pb/U using an in-house MS Excel© spreadsheet program (Gerdes & Zeh, 2006, 2009). A common-Pb correction based on the interference- and background-corrected ^{204}Pb signal and a model Pb composition (Stacey & Kramers, 1975) was carried out (for details see Gerdes & Zeh, 2009). For the analyzed sample the calculated common ^{206}Pb contents was mostly <2.0% (for most concordant grains <0.8%) of the total ^{206}Pb but in very rare cases exceeded 10% (Table S1; Heubeck, Thomsen, et al., 2022). Laser-induced elemental fractionation and instrumental mass discrimination were corrected by normalization to the reference zircon GJ-1 (Jackson et al., 2004). Prior to this normalization, the inter-elemental fractionation ($^{206}\text{Pb}^*/^{238}\text{U}$) during the 21 s of sample

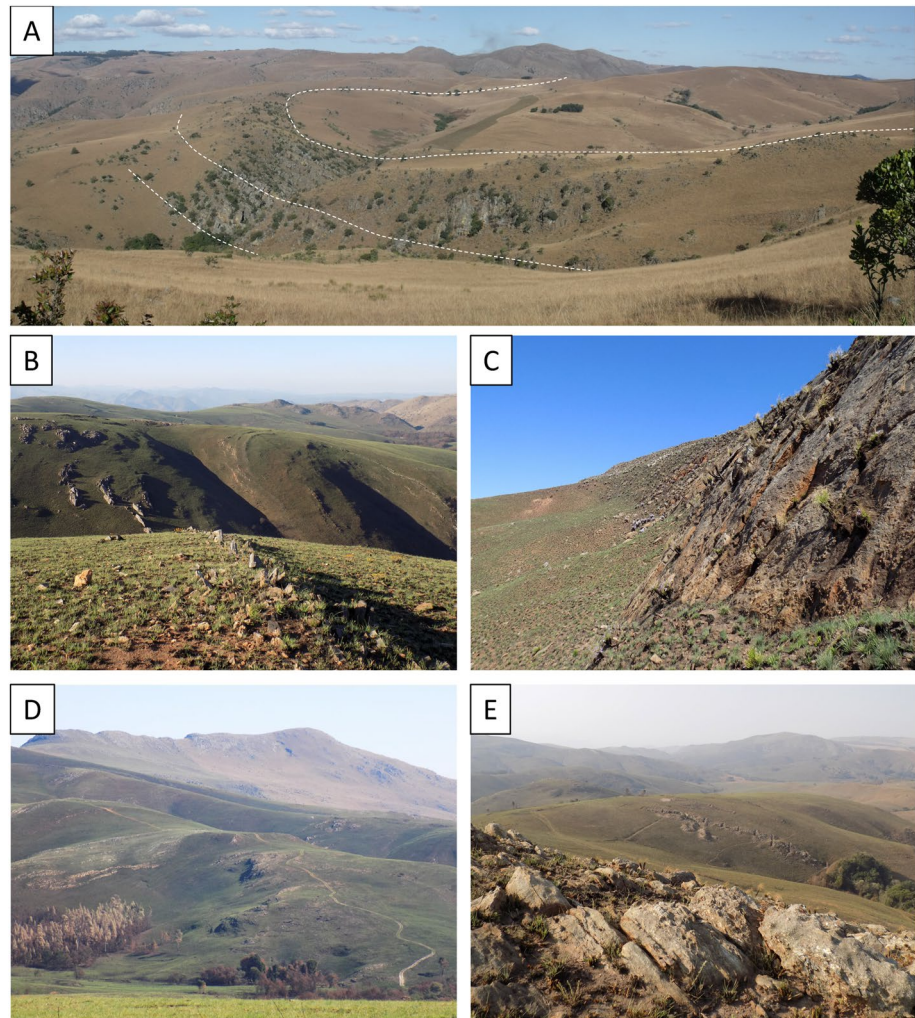


Figure 3. Malolotsha Syncline geology. (a) Hinge of Malolotsha Syncline in the middleground. Resistant Moodies Group sandstones dip to the right and define fold plunge; they are overlain by soft talc schists of the Onverwacht Group. (b) Synform defined by chert bands and foliated talc schists in the central Malolotsha Syncline. View is to the north. (c) Bedding-parallel thrust-fault contact between Moodies Group quartzose (meta-)sandstones (right) and Onverwacht talc schists (left). View is to the south. (d) View westward across talc schists laced with tightly folded chert bands (cp. Figure 2) in the core of the Malolotsha Syncline; Moodies Group sandstones of the western limb in the background dip toward the viewer. (e) View northeastward from upward-facing, interbedded sandstones and conglomerates at the top of the Moodies Group in the western limb of the Malolotsha Syncline (Site CH 19–127) toward abandoned trenches of Emerald Mine in Onverwacht talc schists in the middleground.

ablation was corrected for each individual analysis. The correction was done by applying a linear regression through all measured, common Pb corrected ratios, excluding the outliers (± 2 SD), and using the intercept with the y-axis as the initial ratio. The total offset of the measured drift-corrected $^{206}\text{Pb}^*/^{238}\text{U}$ ratio from the reported (“true”) ID-TIMS GUF value (0.0983 ± 0.0004) of the analyzed GJ-1 grain was between 4% and 7% during the analytical session. Reported uncertainties (2σ) of the $^{206}\text{Pb}/^{238}\text{U}$ ratio were propagated by quadratic addition of the external reproducibility (2 SD) obtained from the standard zircon GJ-1 (see <https://dataservices.gfz-potsdam.de/panmetaworks/review/c80344ba14a46f81478be07ee583519b7167f68244fd9284dc8b44edc17c829b/>) and the within-run precision of each analysis (2 SE; standard error). In case of the $^{207}\text{Pb}/^{206}\text{Pb}$, we used a ^{207}Pb signal dependent uncertainty propagation (see Gerdes & Zeh, 2009). The $^{207}\text{Pb}/^{235}\text{U}$ ratio is derived from the normalized and error propagated $^{207}\text{Pb}/^{206}\text{Pb}^*$ and $^{206}\text{Pb}^*/^{238}\text{U}$ ratios assuming a $^{238}\text{U}/^{235}\text{U}$ natural abundance ratio of 137.818 (Hiess et al., 2012) and the uncertainty derived by quadratic addition of the propagated uncertainties of both ratios. The accuracy of the method was verified by analyses of the reference zircons GJ-1, BB and Plešovice

(Jackson et al., 2004; Santos et al., 2017; Sláma et al., 2008). The results of unknowns and standard measurements are shown in Table S1 (Heubeck, Thomsen, et al., 2022).

At the Geological Survey of Denmark and Greenland (GEUS), a NWR213 solid state Nd:YAG laser system from Elemental Scientific Lasers mounted with a standard TV2 ablation cell was coupled to an Element 2 single-collector magnetic sector-field ICP-MS from Thermo Fisher Scientific. The mass spectrometer is equipped with a Jet interface pump system and used X-type sample and H-type skimmer cones both of Ni, and a quartz torch shielded with a grounded Pt electrode. Operating conditions and data acquisition parameters are listed in Table S1 (Heubeck, Thomsen, et al., 2022). The laser was heated up for at least 15 min before operation, providing stable laser output energy and flat ablation craters by the “resonator-flat” laser beam. Prior to loading, samples and standards were carefully cleaned using ethanol and an ultrasonic bath to remove surface contamination. The ablation cell with the custom-made sample holder was flushed with helium gas to minimize and stabilize the gas blank level. Helium was used as carrier gas and was mixed with argon gas ca. 0.5 m before entering the plasma in the mass spectrometer. The mass spectrometer was run for at least 1 hr before analysis to stabilize and minimize the Hg and Pb background signal. Just before analysis began, the ICP-MS was optimized for dry plasma conditions through continuous linear ablation of the GJ-1 zircon standard. The signal-to-noise ratios for the heavy mass range of interest (i.e., ^{202}Hg to ^{238}U), emphasizing on ^{238}U and ^{206}Pb , were maximized, while keeping oxide production, monitored as $^{254}\text{UO}/^{238}\text{U}$, below <0.2%. To minimize instrumental drift, a standard-sample-standard analysis protocol was followed, bracketing eight zircon analyses by four to six Harvard 91,500 standard zircon analyses (Wiedenbeck et al., 1995, 2004) measurements. For quality control, the GJ-1 (Jackson et al., 2004), Plešovice (Sláma et al., 2008) and Temora-2 (Black et al., 2004) reference zircons were measured regularly during the analysis sequences, all yielding an averaged accuracy of <0.8% deviation compared to published reference values, and an internal averaged precision within 4%–5%. Data were obtained from single-spot analysis using a laser spot size of 25 μm , a pulse rate of 10 Hz, and a nominal laser fluence of ca. 3 J/cm^2 . Acquisition of the single spot analysis included 30 s background measurement followed by laser ablation for 30 s, and washout for 35 s. Factory-supplied software was employed for the acquisition of the transient data, acquired through automated running mode of pre-set analytical locations. Based on CL and BSE images as well as the optical view during analysis, analyses spots on the grains were attempted to be set at inclusion-free locations free of cracks. Data processing and calculation of isotopic ratios and dates were carried out off-line through the software Iolite v. 2.5 (Hellstrom et al., 2008; Paton et al., 2011) using the Iolite-integral VizualAge data reduction scheme by Petrus and Kamber (2012). The VizualAge data reduction scheme includes a correction routine for down-hole isotopic fractionation (Paton et al., 2010) and provides routines for data that require correction for common Pb. All diagrams were produced using IsoPlotR (Vermeesch, 2018, 2021).

We constructed a geological profile across the Malolotsha Syncline based on the geological mapping and unfolded it using Move Modeling Suite software (Petroleum Experts), using its Flexural Slip algorithm (Egan et al., 1997; Tanner, 1989). The unfolded profile served as reference section for 2-D kinematic forward modeling, basing the initial layer-cake model on minimal but constant thicknesses of the Moodies and Onverwacht Group strata inferred from the cross section. Fault depth, position, geometry and the amount of displacement was assessed by trial-and-error individually for five mapped faults to obtain a best fit to the deformed reference section. For kinematic forward modeling, the Fault Parallel Flow (Egan et al., 1997) algorithm was used. Lastly, this forward-modeled imbricate thrust stack was refolded using the Flexural Slip algorithm.

4. Geology of the Malolotsha Syncline

4.1. Talc Schists

Despite their very low resistance to weathering and the resulting subdued topography, talc schists are locally well exposed (in some places continuously over hundreds of m) in numerous stream channels in the core of the Malolotsha Syncline, as well as along tracks, and in legacy exploration trenches across grassland (Figures 3 and 4). Soil cover is widely thin, and low outcrops abound when and where the grass is burned. Lamb (1984, 1986) estimated the thickness of the talc schists to exceed 1 km. They consist of strongly foliated silvery-brown rock made of platelets of fine-grained talc, sericite, carbonate, and serpentinite (Lamb, 1984; Lamb & Paris, 1988; Travers, 2020). Locally, mm- to cm-sized nodules of weathered ferruginous carbonate minerals, possibly ankerite or siderite, are common (Travers, 2020; Figure 4f).

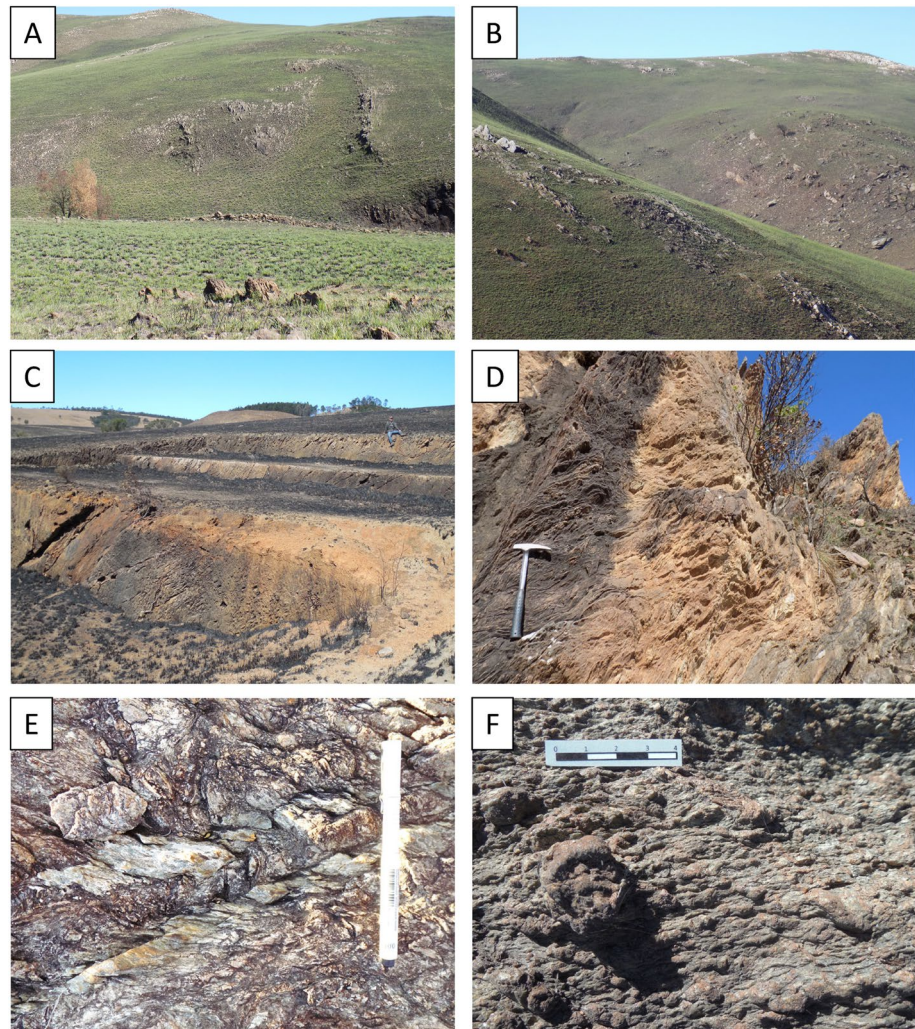


Figure 4. Characteristics of talcose schists of the Onverwacht Group klippe in the core of the Malolotsha Syncline. (a) Tight meso-scale folding in talcose schists; (b) Stacked fold hinges in interbedded cherts and talcose schists; (c) Shooting range quarry, showing steep foliation in talcose schists. Person (upper right) for scale; (d) Crenulated talc schists, former Emerald Mine. Hammer for scale is 43 cm long; (e) Foliated and sheared talc schists; pen is 18 cm in length. (f) Nodular, weakly foliated talc schists. Orange nodules are domains of siderite and dolomite. Scale is 4 cm in length.

4.2. Chert

Talc schists are interbedded with numerous beds, ca. 0.5–20 m thick, of silicified volcaniclastic rocks (cherts) which are traceable for tens to hundreds of m along strike, regionally and locally subparallel to the foliation in the talc schists. They are highly weathering-resistant and morphologically prominent. Many cherts are deformed to tight to isoclinal folds or hinge fragments (Figures 4a and 4b) and are locally offset by minor faults; they are commonly brittily fractured (Figure 5b). The plunge of minor fold axes in the cherts mostly conforms to that of the large-scale Malolotsha Syncline. In places, partial sheath folds are mappable (Figure 4b) whose attitudes deviate from the regional structure moderately.

In outcrop, several varieties of chert can be distinguished (Figure 5): (a) Microcrystalline black-and-white banded chert; (b) gray, very-fine-grained, finely laminated and subtly graded chert; (c) microcrystalline, banded ferruginous chert; (d) gray, silty, normally graded, silicified tuffaceous sandstone with small-scale ripple-drift cross lamination; (e) sedimentary breccias of normally graded, angular, cm-sized lensoid fine-grained volcanic fragments encased in a fine-grained microcrystalline matrix; (f) evenly fine-grained porcelain-colored or pale green silicified tuff; and (g) chert-clast conglomerate in a silicified sandy matrix. Upward-facing directions are rarely identifiable; upper and lower contacts are unexposed.

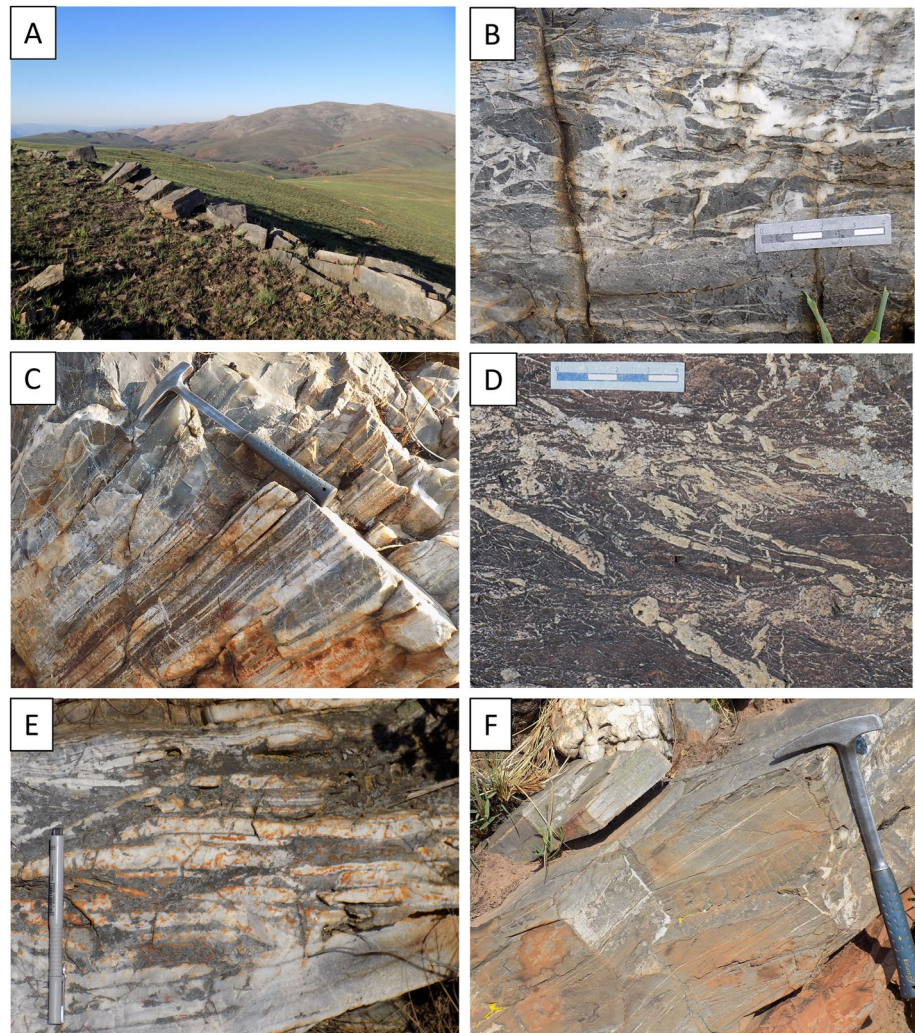


Figure 5. Outcrop appearance of silicified volcanic and volcanoclastic units (cherts) which are interbedded with thick talcose schists in the core of the Malolotsha Syncline. (a) fine-grained, laminated, aqueously reworked gray tuff (site 21–246); (b) sedimentary graded breccia of fine-grained volcanoclastic fragments in white silica matrix (site 19–134); (c) banded black-and-white chert (site 19–120); (d) silicified matrix-supported slab conglomerate in fine-grained matrix (site 16–230); (e) clast-supported slab conglomerate in fine-grained matrix (site 18–269); (f) homogenous very-fine-grained tuff (site 19–121).

Due to the structural complexity and lensoid character of the cherts, we could not construct a stratigraphic sequence within the chert-laced talc schists. Lamb (1984) identified nine units, some of which are separated by discrete planar shear zones. The occasional abrupt termination of chert units on map-scale suggested to Lamb (1984) that major faults within the talc schists modify an original stratigraphic sequence of approximately several hundred meter original thickness (Figure 2).

4.3. Quartzose Sandstones

Limbs and hinge region of the Malolotsha Syncline are composed of km-thick, quartz-dominated, mostly silicified, well-sorted sandstones (Figure 6; Lamb, 1984; Lamb & Paris, 1988). Grain size is dominantly medium but coarse-grained units are widespread, commonly grading into granuly and gravelly sandstones. Thin lensoid conglomerates are rarely interbedded with sandstone units; they are more common to the south. Shales (metamorphosed to schists) occur only as drapes on rippled bedding planes and foresets (Figure 6a). Sandstones are medium- to thick-bedded and show abundant sedimentary structures indicative of shallow-water deposition,

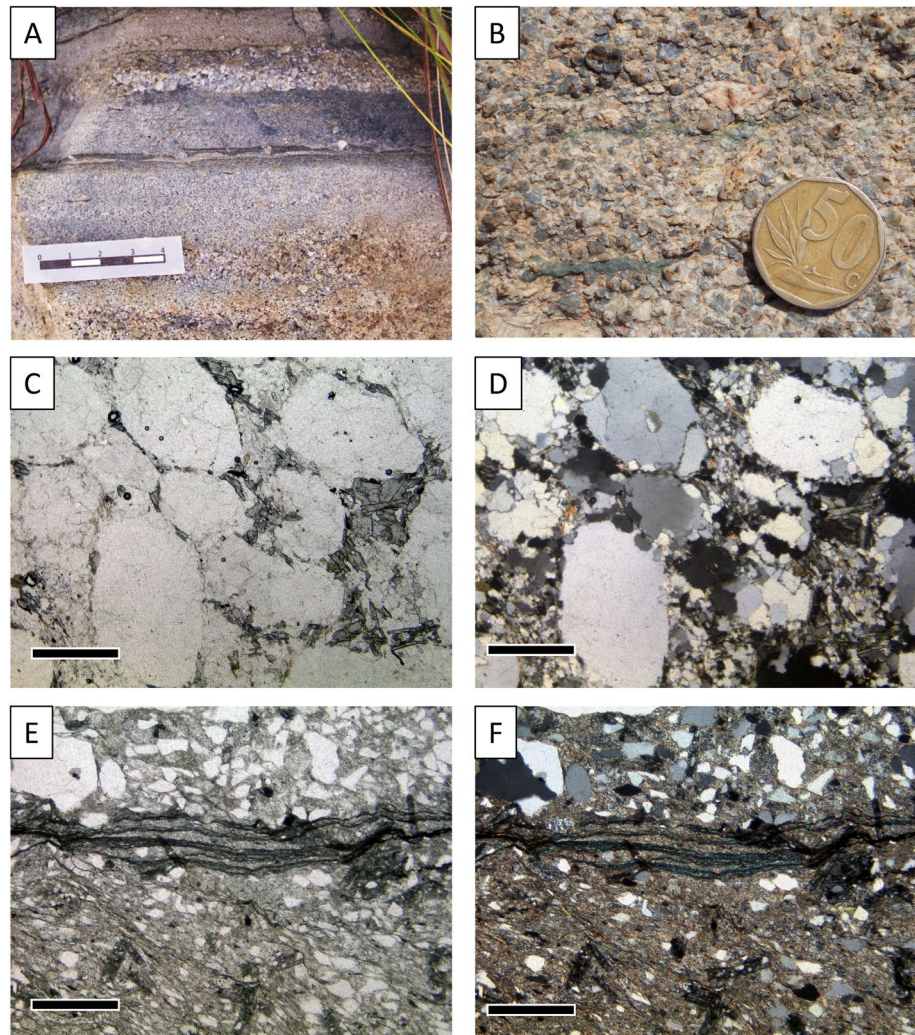


Figure 6. Characteristics of Moodies Group sandstones. (a) Mudcracked shale laminae interbedded with granuly to fine-grained sandstones; scale is 4 cm long; (b) granuly sandstone with green fragment of ultramafic volcanic rock; coin is 21 mm in diameter; (c–f) Moodies sandstones in thin section. Scale bar is 200 μm long. Left: Plane light; right: Polarized light; (c, d) very-coarse-grained sandstone. Large monocrystalline quartz grains in quartzose-sericite matrix have undergone polygonization and grain-to-grain suturing; (e, f) Fine-grained sandstone with micaceous former shale lamination. Stratigraphic younging is up. Note common radial chloritoid clusters.

including ubiquitous horizontal bedding, low-angle cross-bedding, planar and trough cross-bedding, ripple marks, shale drapes on rippled bedding planes, desiccation cracks in shale laminae, and shallow erosional scours. Mud chips, rip-up clasts and fluid-escape structures are rare (cp. Lamb & Paris, 1988). The stratigraphically-up facing direction can be established readily in many places. It is always structurally inwards, that is, toward the core of the syncline.

Sandstone framework grains are well to poorly sorted and appear mostly subangular in hand sample (Figure 6b); they consist of dominant water-clear quartz, off-white fine-grained altered feldspar and quartz-sericite-mosaic mineral grains, and black chert (Figures 6c–6f). Conglomerate clasts are dominated by white, gray and black chert varieties, with subordinate pale-yellow feldspar porphyry and rare green altered ultramafic rock, which is a common combination of Moodies conglomerates clasts throughout the BGB (Heubeck & Lowe, 1999). In thin section, sandstones show a strongly recrystallized mosaic of dominant quartz and coarsely recrystallized quartz-sericite grains, locally interbedded with thin seams of carbonaceous matter (Figure 6). Grain-to-grain contacts are linear or sutured.

Several thin, bedding-parallel, grassy strips tens of m wide and several hundred m to several km long, underlain by poorly exposed talc schists, are interleaved in this seemingly nearly monotonous siliciclastic sequence, in particular in the structurally thickened hinge zone of the Malolotsha Syncline (Figure 2). The Geological Survey of Swaziland (1970) and Lamb (1984, 1986) interpreted these strips as marking bedding-parallel major fault planes along which structural duplication had taken place.

4.4. Metamorphic Grade

Although the overall grade of metamorphism in the Moodies Group is lower greenschist-facies, multiple regional alteration events have affected the greenstone belt in the Archean and Palaeoproterozoic during burial, including aqueous alteration and thermal events. Virtually all BGB rocks have been altered at temperatures in excess of 300°C (Cloete, 1999; Heubeck, Drabon, et al., 2022; Heubeck, Thomsen, et al., 2022; Reimann et al., 2021; Tice et al., 2004; Toulkeridis et al., 1998; Xie et al., 1997). Mineral alteration, ductile strain and metamorphic grade differ regionally; in the Malolotsha region, they increase toward the BGB margin to the southeast.

Thin Moodies Group siltstones and thin metapelites on the limbs of the Malolotsha Syncline limbs contain common metamorphic chloritoid (Figure 6f). The presence of chloritoid is rather non-specific, indicating temperatures between 220°C, which marks the chloritoid-in reaction in Fe-rich metapelites (this temperature is somewhat higher in “normal” metapelites), and 550°C, which represents the chloritoid-out reaction (Bucher & Frey, 1994; Ganguly, 1969).

4.5. Previous Age Dating

Lana et al. (2011; their sample W23) dated a foliated amphibolite 10 km to the northeast of the Malolotsha Syncline, separated from it by the tight, highly deformed Forbes Reef (or Malolotsha) Anticline by several imbricated fault slivers and without mappable connection to the Malolotsha Syncline core of talc schists. Its interpreted crystallization age of $3,419 \pm 10$ Ma is 100 Ma older than the inferred sedimentation ages we discuss from detrital zircons in the silicified volcanoclastic sandstones, siltstones and tuffs below.

Three sets of age estimates represent detrital zircon data from Moodies Group strata in Eswatini:

1. A sandstone sample in the northern hinge region of the Malolotsha Syncline (sample 13–351 of Heubeck, Drabon, et al., 2022) yielded only eight zircon mineral grains of which six grains passed the quality criteria (concordance 85%–106%, $U < 400$ ppm, 2 SD of the $^{207}\text{Pb}/^{206}\text{Pb}$ date < 40 Ma; Heubeck, Drabon, et al., 2022; Heubeck, Thomsen, et al., 2022). The low number of grains prevents a statistical assessment of the maximum depositional age. Three grains 104%, 95%, and 87% concordant, yielded discordia-intercept age of $3,227 \pm 31$, $3,211 \pm 33$, and $3,232 \pm 31$ Ma. Two grains (86% and 102% concordant) yielded ages of $3,420 \pm 32$ and $3,448 \pm 30$ Ma, respectively. One grain (102% concordant) had an age of $3,274 \pm 31$ Ma.
2. An aqueously reworked metatuff interbedded with thick Moodies sandstones in the northern Malolotsha area (sample 13–342 of Heubeck, Drabon, et al., 2022; Heubeck, Thomsen, et al., 2022; $n = 62$; Wiechert, 2014) lacked young grains and indicated a maximum depositional age of 3,250 Ma.
3. Detrital zircon dates from the matrix of the Moodies basal conglomerate of the Ntaba Mhlope Syncline (sample 16–226 of Heubeck, Drabon, et al., 2022; Heubeck, Thomsen, et al., 2022; $n = 26$), ca. 22 km along strike to the northeast, show an age spectrum consistent with an onset of Moodies deposition at ca. $3,235 \pm 15$ Ma.

The spectrum of zircon dates in Moodies Group tuffs is often complex because the zircon population commonly includes xenocrysts of various ages incorporated during magmatic processes and because detrital zircons are admixed to the tephra during post-eruptive aquatic transport. The age information of this grain mixture is then usually modified by several Late Archean metamorphic and tectonothermal events and Recent weathering which reset part of the population (Heubeck, Drabon, et al., 2022; Heubeck, Thomsen, et al., 2022). However, the three DZ dates spectra from the region all resemble the Moodies detrital zircon spectra from South Africa. The current small database does not provide enough resolution to support a postulated diachronous onset of Moodies sedimentation in the southern BGB (de Wit, 1991).

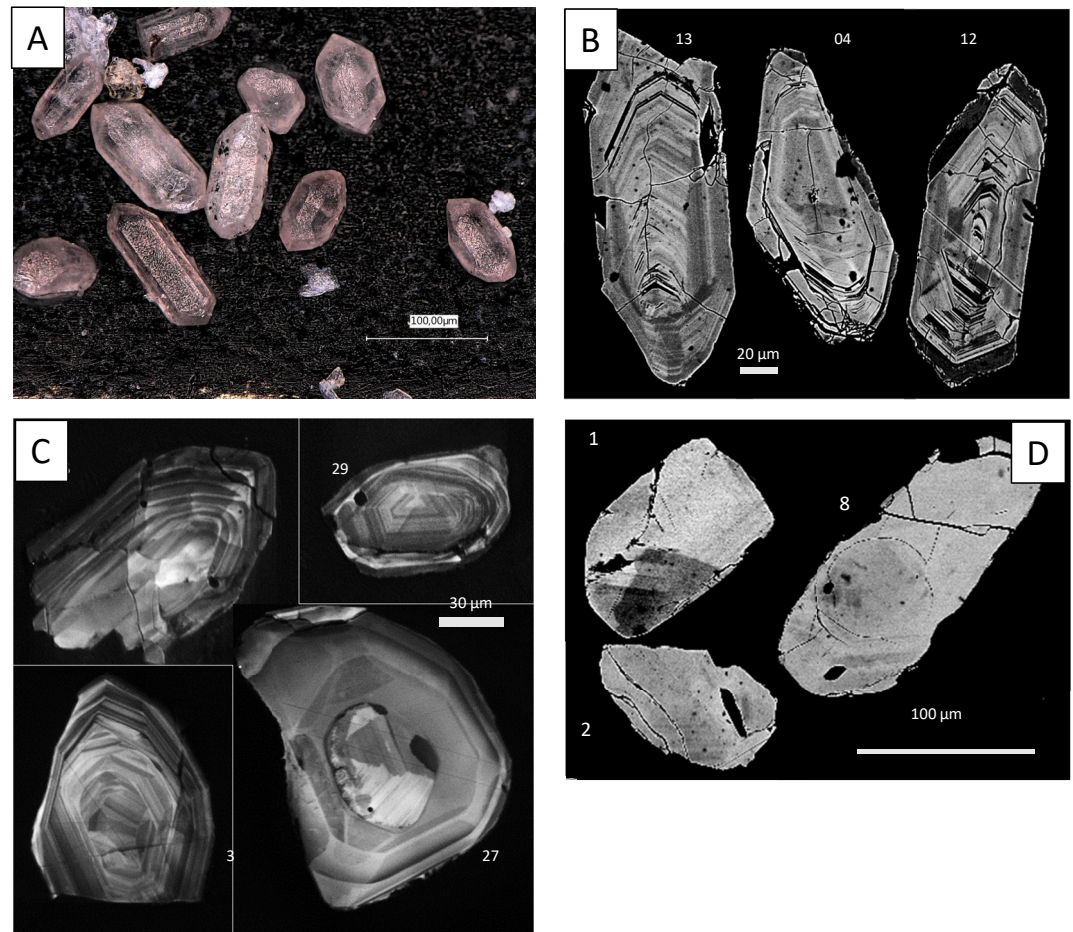


Figure 7. SEM and BSE images of dated zircon populations. (a) Close-up photograph of bipyramidal zircons of sample 18–270; (b) HDBSD images of zircons (sample 19–133); grain numbers indicated; (c) Cathodoluminescence images of the 100% and 101% concordant zircons used for precise dating of sample 19–130; (d) HDBSD images of representative dated zircons of sample 19–122.

5. Results

5.1. Zircon U-Pb Dating

Sample 18–270 (Table S1; Heubeck, Thomsen, et al., 2022) was taken from a weathering-resistant chert unit ca. 300 m above the contact between underlying quartzose sandstones and overlying talc schists in the west-central Malolotsha Syncline. The chert unit, ca. 3 m thick, is a homogenous-appearing recrystallized fine-grained rock, possibly an ash-fall tuff. Processing yielded 97 stubby, clear to white bipyramidal zircon grains (Figure 7a) with a mean length of 85 μm ($n = 34$); all 97 grains were dated. Of those, nine grains passed the quality criteria of $\pm 2\%$ concordance, $U < 400$ ppm, and 2 sigma < 20 Ma, yielding a weighted mean $^{207}\text{Pb}/^{206}\text{Pb}$ date of $3,291 \pm 13$ Ma (MSWD = 7.5; Figure 8a). Of the nine zircon grains, seven 100% concordant grains yield a slightly more precise weighted mean $^{207}\text{Pb}/^{206}\text{Pb}$ date of $3,300 \pm 10$ Ma (MSWD = 4.1), and the three youngest fully concordant grains yielded a slightly more precise mean weighted $^{207}\text{Pb}/^{206}\text{Pb}$ date of $3,282 \pm 7$ Ma (Figure 8a).

Sample 19–122 (Table S1; Heubeck, Thomsen, et al., 2022) is a prominent chert in grasslands of the southern Malolotsha Syncline. It represents a partly desilicified, ca. 9–11 m thick fining-upward sedimentary sequence from basal angular, very-coarse-grained volcanic fragments grading upward into gray, thin-bedded and laminated cherty siltstone, overlain by gray-and-white-banded chert. The sample yielded 13 dated grains of which 10 passed the quality criteria of $U < 350$ ppm, $99 < \text{concordance} < 101\%$, and 2 sigma < 15 Ma. Their weighted mean $^{207}\text{Pb}/^{206}\text{Pb}$ date is $3,330 \pm 4$ Ma (MSWD = 4.3); a concordia upper-intercept age on the same grain subset

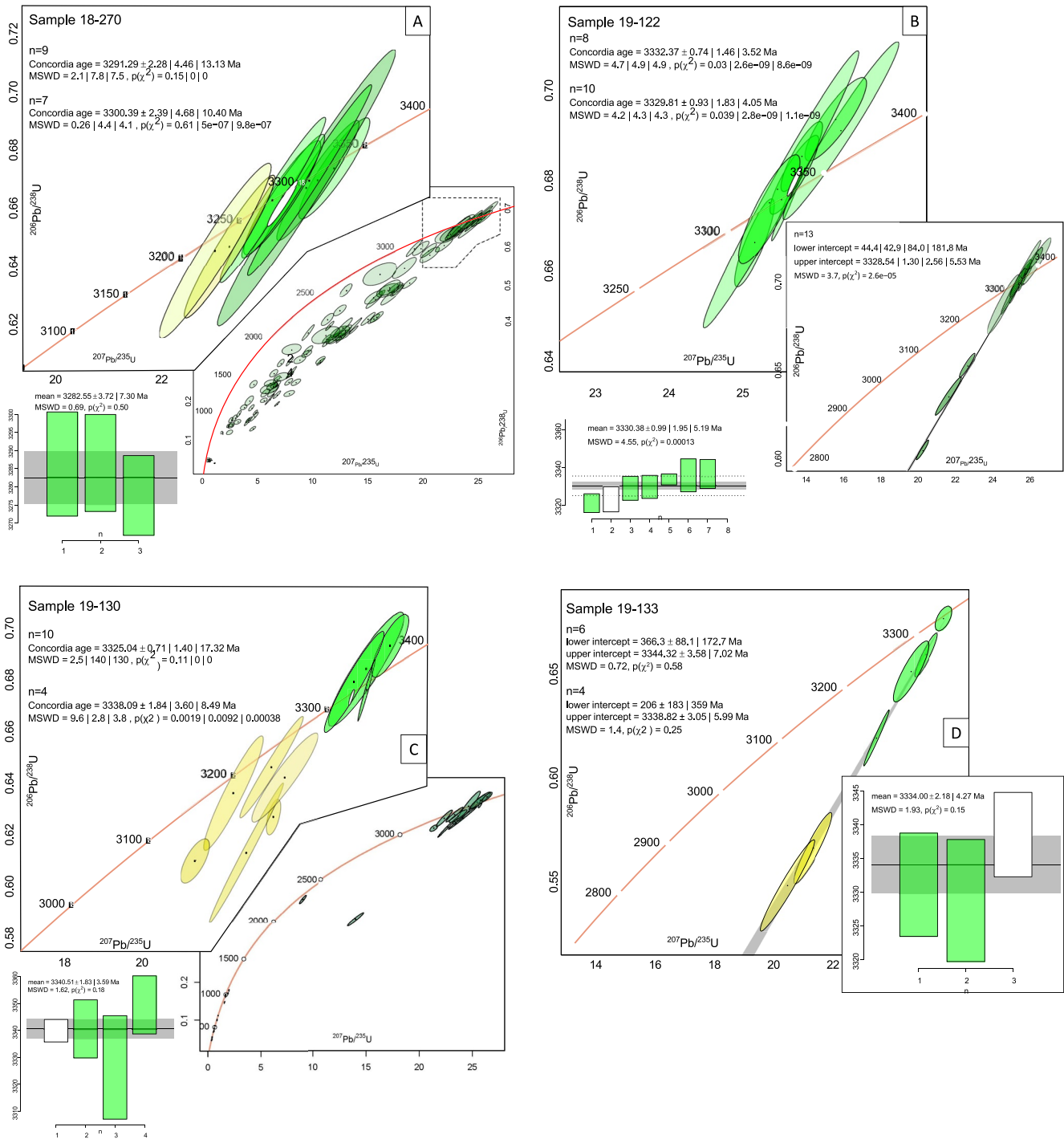


Figure 8. (a–d) Concordia age diagrams of dated zircons from chert units in the core of the Malotsha Syncline. The most concordant zircons from the group passing the selection criteria are shown in green. See text for discussion. Data are in Heubeck, Drabon, et al. (2022), Heubeck, Thomsen, et al. (2022). (a) Concordia age diagrams of dated zircons of sample 18–270. Only nine of the 97 dated grains passed the selection criteria (see text). The concordia date of those nine grains is $3,291 \pm 13$ Ma, of the most concordant seven grains $3,300 \pm 10$ Ma, and a weighted mean $^{207}\text{Pb}/^{206}\text{Pb}$ date of the youngest three 100% concordant grains $3,282 \pm 7$ Ma. (b) Concordia age diagrams of dated zircons of sample 19–122. Concordia-intercept date of all 13 dated grains is $3,329 \pm 6$ Ma, of the most concordant eight grains $3,332 \pm 4$ Ma, and a mean weighted $^{206}\text{Pb}/^{207}\text{Pb}$ age of the seven 99%–101% concordant grains $3,330 \pm 5$ Ma. (c) Concordia age diagrams of dated zircons of Sample 19–130. An imprecise concordia-intercept date based on the 10 grains passing the selection criteria is $3,325 \pm 17$ Ma, of the four most concordant grains $3,338 \pm 8$ Ma, and a mean weighted $^{206}\text{Pb}/^{207}\text{Pb}$ age of the four most concordant grains is $3,341 \pm 4$ Ma. (d) Concordia age diagram of dated zircons of sample 19–133. The concordia-intercept date of the six grains meeting the selection criteria is $3,344 \pm 7$ Ma, of the four most concordant grains $3,339 \pm 6$ Ma. A weighted mean $^{207}\text{Pb}/^{206}\text{Pb}$ date of the three most concordant grains yields a date of $3,334 \pm 4$ Ma.

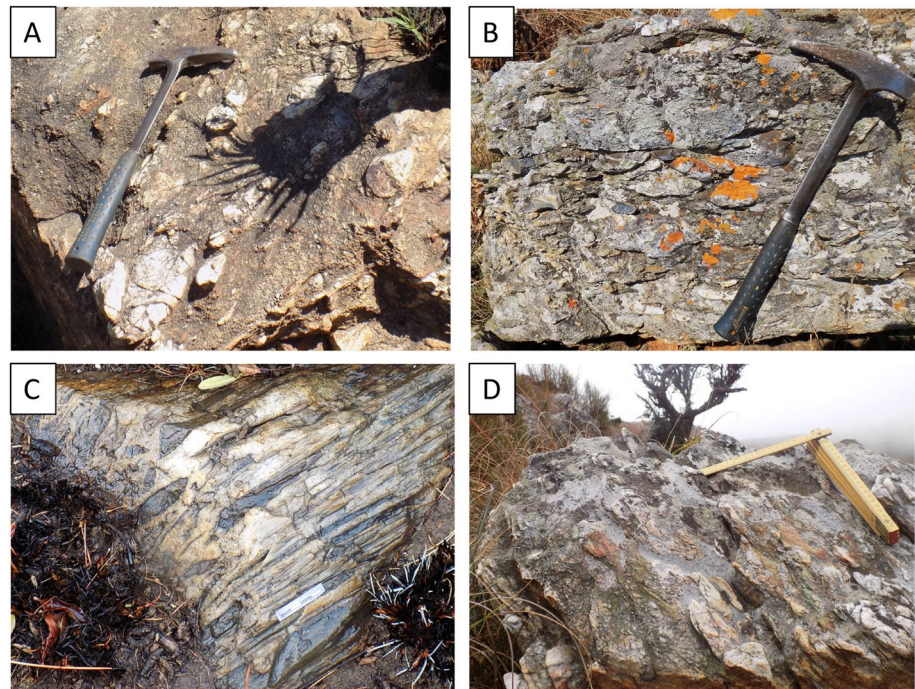


Figure 9. Strain markers in outcrop. (a) Gravelly sandstone near the contact of Moodies Group to overlying talc schists. Hammer (41 cm long) lies on a steeply dipping bedding plane and is oriented in the direction of maximum clast elongation; loc. 21–242; (b) Moderately flattened conglomerate clasts on the western limb of Malolotsha Syncline; (c) Strongly rodded and flattened chert-clast conglomerate near the core of the Malolotsha Syncline, over- and underlain by talcose schists; loc. 85; (d) Strongly flattened and elongated Moodies conglomerate clasts ca. 100 m west of the contact of the BGB with the high-grade gneisses of the Malolotja Inlier, part of the Ancient Gneiss Complex. View is northward along strike, bedding dips to the right. Scale is 20 cm long; loc. 101.

an identical date of $3,329 \pm 5$ Ma. The weighted mean $^{207}\text{Pb}/^{206}\text{Pb}$ date of the seven grains 99%–101% concordant yield an identical date of $3,330 \pm 5$ Ma (MSWD = 4.55; Figure 8b).

Sample 19–130 (Table S1; Heubeck, Thomsen, et al., 2022) was taken from the matrix of a highly strained chert-clast conglomerate in the hinge region of the northern Malolotsha Syncline (Figures 8c and 9c). Out of 31 analyzed zircons, 10 zircons passed the quality criteria of $U \leq 400$ ppm, $96 < \text{concordance} < 101$, and $2 \text{ sigma} < 20$ Ma, yielding an imprecise weighted mean $^{207}\text{Pb}/^{206}\text{Pb}$ date of $3,325 \pm 17$ Ma (MSWD = 130; Figure 8c). Of those 10 grains, four grains 101% and 100% concordant yielded a combined, more precise concordant date of $3,338 \pm 8$ Ma (Figure 8c); the same four grains yielded a slightly more precise mean weighted $^{207}\text{Pb}/^{206}\text{Pb}$ date of $3,341 \pm 4$ Ma.

Sample 19–133 (Table S1; Heubeck, Thomsen, et al., 2022) was taken from a sheath-folded chert unit showing a nearly circular outcrop pattern in the west-central Malolotsha Syncline (Figure 2). The chert is a silicified, fining-upward unit of dark gray, angular, granule-sized volcanic fragments within a white chert matrix, overlain by black-and-white banded and gray laminated chert (Figure 5b). A bed of fine-grained white chert yielded 14, in part significantly discordant grains which yielded an upper-intercept $^{207}\text{Pb}/^{206}\text{Pb}$ date of $3,341 \pm 18$ Ma. Of those, the six grains passing the quality criteria of $U < 300$ ppm, $90 < \text{concordance} > 100$, and $2 \text{ sigma} < 20$ Ma yielded a concordia upper-intercept date of $3,344 \pm 7$ Ma (MSWD = 0.72; Figure 8d). Of those six grains, the four most concordant grains, 96%, 98%, 98%, and 100% concordant, yielded a concordia upper-intercept age of $3,339 \pm 6$ Ma, and the three most concordant grains yielded a slightly more precise weighted mean $^{207}\text{Pb}/^{206}\text{Pb}$ date of $3,334 \pm 4$ Ma (MSWD = 1.93).

5.2. Strain

Strain in the Malolotsha Syncline is represented by the reorientation of platy minerals in the talc schists, forming a pronounced and ubiquitous foliation, and by deformed pebbles and cobbles in gravelly sandstones and thin

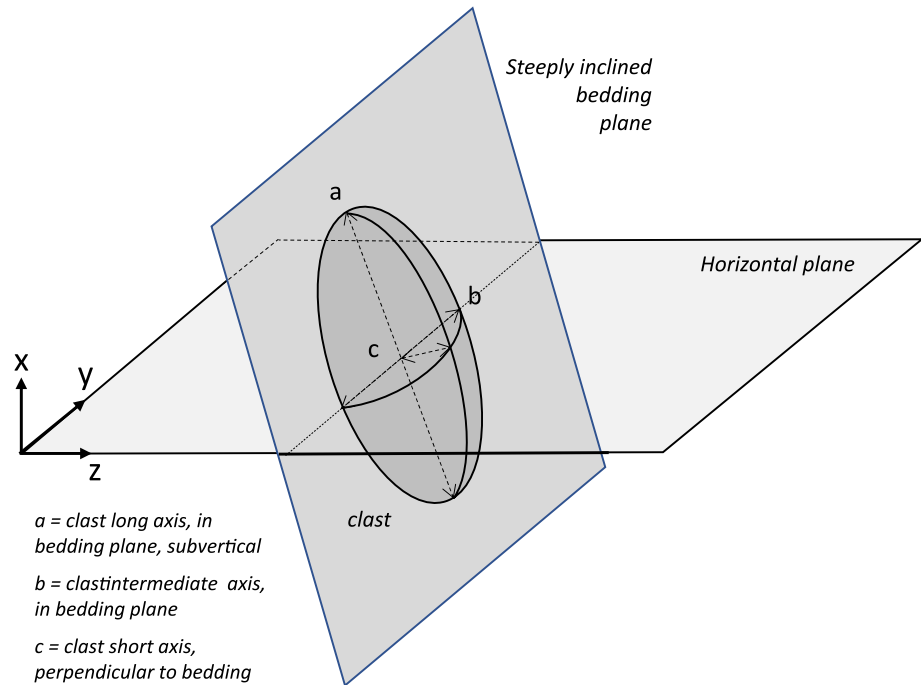


Figure 10. Naming conventions used in clast diameter orientations and strain ellipsoid axes. Map (Figure 12) shows *yz*-ellipsoids; cross section (Figure 13) shows *xz*-ellipsoids.

conglomerates, defining a penetrative lineation (Table S2; Heubeck, Thomsen, et al., 2022). The latter data type provides the opportunity to estimate the magnitude, type and orientation of regional ductile strain. The very large competence contrast between the highly competent quartzose sandstones on the limbs of the Malolotsha Syncline and the extremely incompetent talc schists in its core, combined with the tight folding and imbricate faulting, produced a highly heterogeneous strain pattern.

Cursory inspection of sedimentary structures in outcrops of quartzose Moodies Group (meta-)sandstones shows little apparent strain. Measurements of clast populations near the faulted contacts of Moodies sandstones to the structurally overlying talc schists, however, show that strain is moderate to high within a ca. 50–100 m wide contact zone in the sandstones (Figures 9a and 9b). Strain also increases in magnitude south-eastward near the complex, sheared intrusive contact of the BGB to the Piggs Peak batholith where the tight, structurally strained Forbes Reef Anticline separates the Malolotsha Syncline from high-grade metamorphic rocks of the Malolotja Inlier, part of the AGC, and the intrusive contact with the Piggs Peak batholith (Lamb, 1984; Schoene & Bowring, 2010; Figure 9d). Strained gravelly sandstones and conglomerates at nearly all surveyed locations are *L-S* tectonites, with $L > S$, indicating a significant proportion of constrictional strain (Figures 9–11). Clasts are flattened in the plane of bedding; their long axes are stretched approximately in the dip direction, perpendicular to strike (Figures 9a and 9d; Figure 10). The orientation of maximum elongation in map view is toward the NW, approximately perpendicular to the present-day SW-NE-trending margin of the BGB (Figure 12; inset).

Cherts interbedded (and likely structurally interleaved) with the talc schists appear in many places un- or minimally strained, with primary sedimentary structures such as current lamination, ripples, grading etc. recognizable. Lapilli are moderately flattened; ripple-drift cross-lamination is significantly flattened in outcrop. Most cherts beds are also highly disrupted by brittle faults with small offsets, veining, and fracturing.

In a few locations, in particular near the contact of the talc schists to structurally underlying Moodies sandstones, cherts appear to show high strain, but its magnitude could be quantified only in a single location in the northern syncline core region (Figure 9c; loc. 85 in Figure 12) where a silicified chert-clast conglomerate records high constrictional strain.

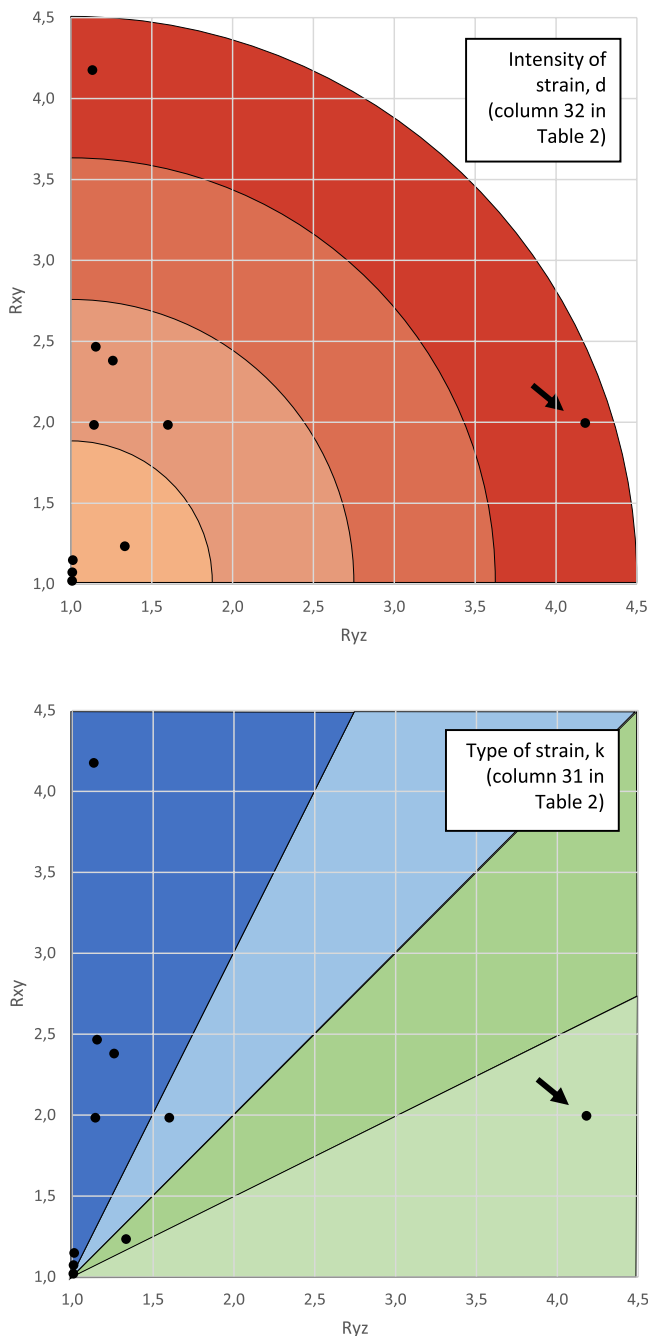


Figure 11. Flinn diagrams of strained conglomerate clasts. Nine clasts are of Moodies Group conglomerate. The single sample from a chert-clast conglomerate interbedded with talc schists shows high flattening strain (arrow), all other clasts show constrictional strain.

Strain in the talcose schists is likely far higher than in the comparatively lightly deformed Moodies strata (cp. Figure 6). Axial planar cleavage and foliation in the talc schists is pronounced and defined by alignment of platy minerals, mostly talc, sericite, and locally serpentinite (Lamb, 1987). Foliation parallels lithologic and structural contacts; it appears to locally steepen toward the core of the Malolotsha Syncline. Fold axes and fold axial planes of crenulation cleavage show the same trend and plunge as the map-scale structure (Lamb, 1984; Travers, 2020). Minor shear zones abound in many outcrops.

5.3. Tectonic Reconstruction

Best-fit kinematic forward modeling of the Malolotsha area along the line of cross-section (Figures 2, 12, 13a, and 13b) shows a northwestwardly-forward-propagating imbricate thrust stack along formerly northwest-vergent faults, followed by tight folding of the stack. In the leading (western) edge of this stack, four faults (numbered 2 through 5 in Figure 13c) repetitively displace thin, ca. 100 m thick slivers consisting of upper Onverwacht and overlying Moodies Group strata along flat-ramp-flat segments. In contrast, a ca. 1,450 m-thick segment of Onverwacht Group strata was detached and thrust on top of ca. 920 m-thick Moodies Group strata along Fault 1 in the east, forming the structurally highest level of the thrust stack in the core of the Malolotsha Syncline (Figures 13c and 14).

6. Discussion

6.1. Age of the Hanging-Wall Sequence; Nature of Zircon Population

The highest-quality zircon clusters from each of the four dated samples yield well-defined concordant or upper intercept $^{207}\text{Pb}/^{206}\text{Pb}$ dates between $3,341 \pm 4$ (sample 19–130) and $3,283 \pm 7$ Ma (sample 18–270). We interpret these dates as an age reflecting crystallization of auto-/antecryst zircons immediately prior to and/or during major felsic to intermediate volcanic eruptions. Eruptions resulted in deposition of effusive and pyroclastic strata, in part from turbulent ash clouds. Older zircon populations are associated to xenocrysts picked up in the magma chamber, the conduit, or during eruption, or are detrital zircon grains admixed to the pyroclastic rocks during subsequent aquatic reworking. The volcanoclastic deposits were silicified early and underwent little if any compaction. Some zircons were reset during subsequent magmatic or tectonothermal events, which is commonly observed in detrital samples throughout the BGB (Heubeck, Drabon, et al., 2022; Heubeck, Thomsen, et al., 2022; Zeh et al., 2013). The structural complexity of the talc schist unit in the core of the Malolotsha Syncline does not allow to recognize a chronostratigraphic order.

6.2. Stratigraphic Correlation

Reported ages, lithologic composition and overall thickness of the strata in the core of the Malolotsha Syncline compare favorably with the uppermost units of the Kromberg and the overlying Mendon formations (Byerly, 1999; Byerly et al., 1996; Decker et al., 2015; Lowe, 1999; Lowe & Byerly, 1999; Thompson Stiegler et al., 2010). Three of the four zircon samples (sample 18–270 is ca. 30 Ma younger; $3,283 \pm 7$ Ma; Figure 8a) have overlapping ages at 3,336 Ma, identical with the age of the Footbridge chert of $3,334 \pm 3$ Ma (Lowe &

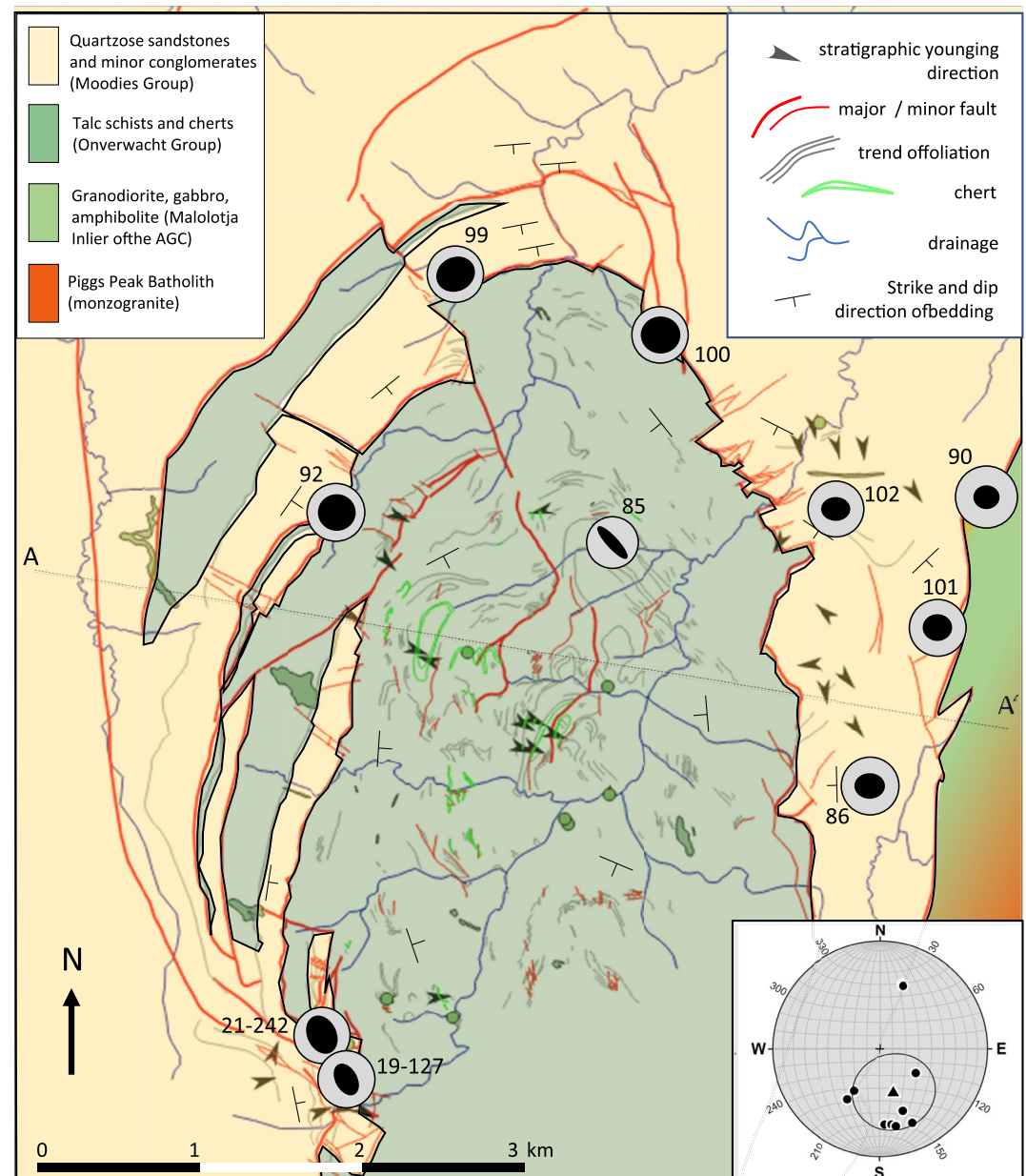


Figure 12. Strain map of the Malolotsha Syncline. Nine yz-strain ellipsoids, derived from clasts of Moodies conglomerates, show subvertically oriented, moderate to high constrictional strain. Numbers refer to locations in Table S2 (Heubeck, Thomsen, et al., 2022). The single conglomerate interbedded with talc schists in the core of the syncline (loc. 85) shows strong flattening strain. The mean orientation of clast long axes is $161/55^\circ$ (inset; triangle).

Byerly, 1999), uppermost unit of the Kromberg Formation (Byerly et al., 1996, 2019). At its type locality along the Komati River in South Africa, this unit is a black and white banded chert ca. 12 m thick (Byerly et al., 1996) which corresponds well to the lithology of several undated chert bands. Our age of $3,283 \pm 7$ Ma of sample 18–270 is only a few Ma younger than a felsic tuff in M2c (a shorthand for the second chert in the Mendon Formation) dated by Byerly et al. (1996) at $3,298 \pm 3$ Ma (sample SA 167, described in Byerly & Palmer, 1991).

Strata of Kromberg and Mendon age are undocumented in the southern part of the BGB (Byerly et al., 2019; Lowe & Byerly, 2007; Lowe et al., 1999) but occur widely in the central BGB north of the Onverwacht Anticline and south of the Inyoka Fault. They are presently best developed in the Umuduha Block of the central BGB

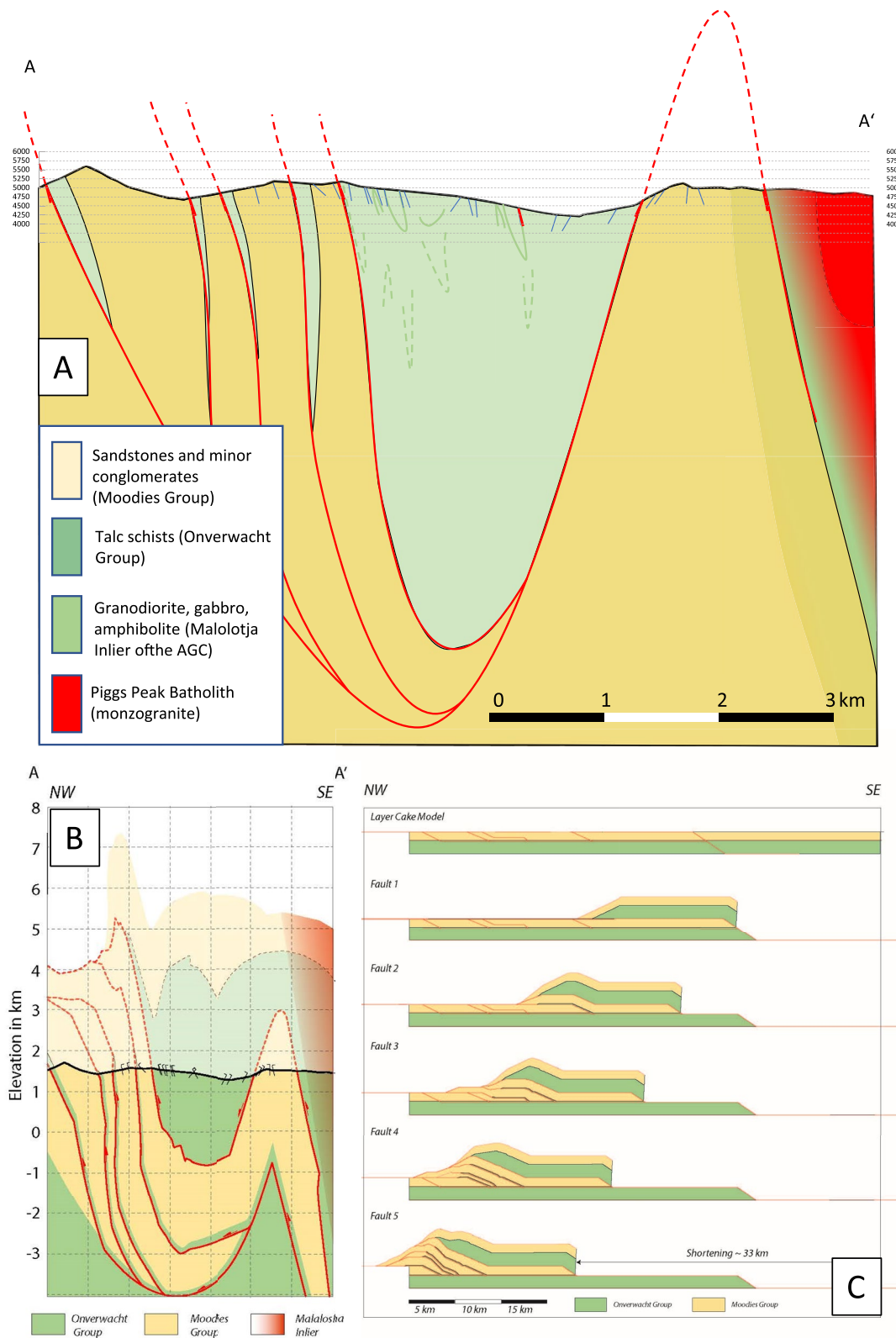


Figure 13.

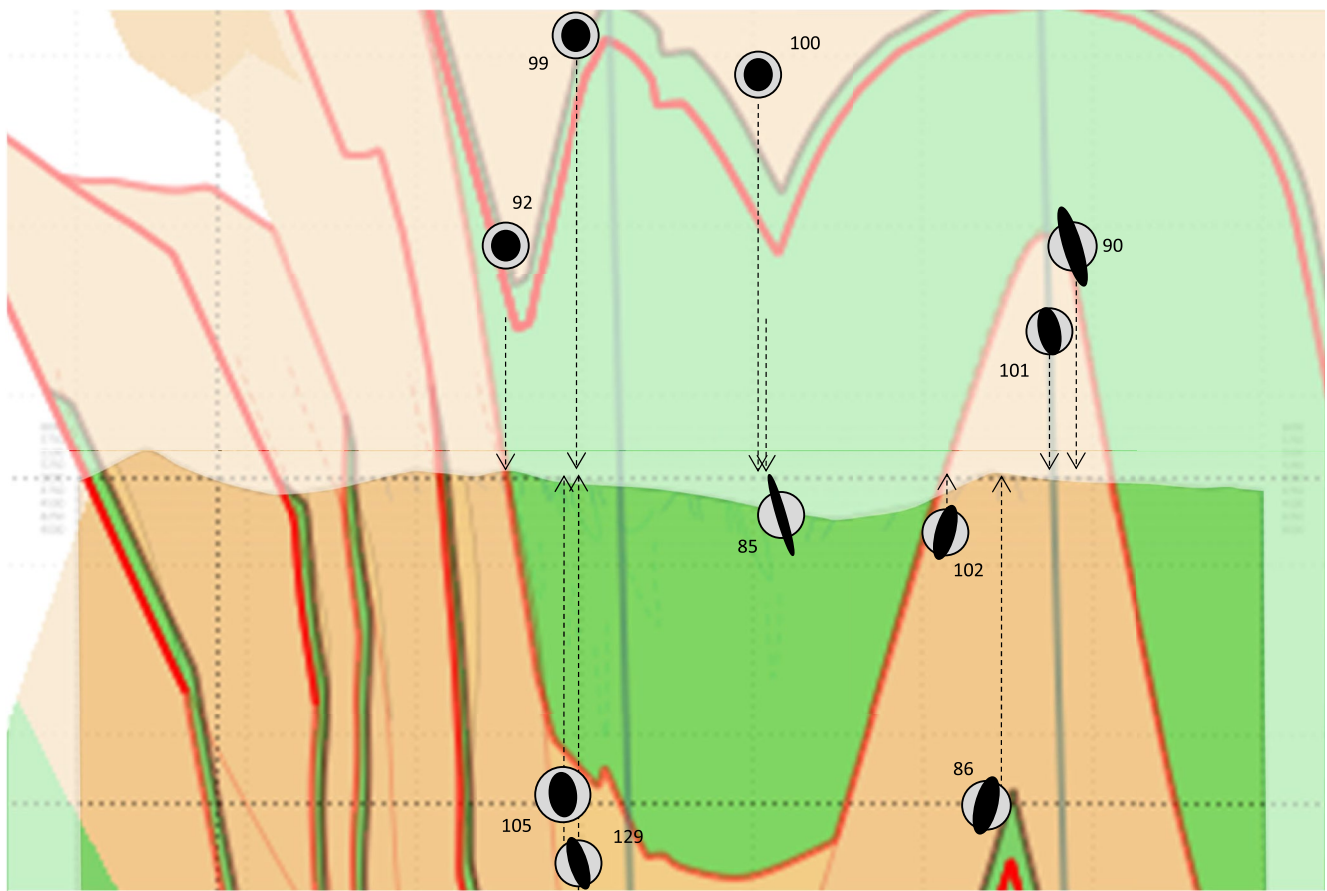


Figure 14. Detail of retrodeformable (balanced) cross section along cross section A-A' in Figure 12b, showing xz -strain ellipsoids. The cross section is extended into the air so that data from up-plunge locations can be projected into the line of section; they show moderate to strong flattening strain.

(Byerly et al., 2019; Lowe et al., 1999); however, because these strata represent volcanism and deposition on one or several large submarine volcanic plateaus, it is likely that Kromberg and Mendon Formation strata extended far beyond the present-day margins of the BGB prior to D4 and D5 deformation.

6.3. Strain

The regional geological context does not support the formation of constrictional strain near ballooning diapirs, major strike-slip shear zones or fold hinges. Strain appears highest along the bedding-plane-parallel, older-over-younger tectonic contacts between Moodies Group sandstones and overlying talc schists and supports an origin by transport-parallel elongation and channel flow along stacked ductile shear zones in which local asperities or thrust ramps developed. Subsequent tight folding of the thrust stack into the Malolotsha Syncline and adjacent fold structures (Lamb, 1984, 1986) may have added flattening strain. In addition, strain partitioning may also have played a significant role by preferentially partitioning simple shear into the rheologically weak talc schists, and the constrictional strain into the rheologically much stronger quartzose sandstones.

Figure 13. Retrodeformation diagrams of the Malolotsha Syncline area. (a) W-E cross section across the Malolotsha Syncline; see Figure 12 for line of section. The Malolotsha Syncline is a synclinally folded imbricate stack of Moodies and Onverwacht Group strata; (b) Retrodeformable (balanced) W-E-oriented cross section of panel a. The thrust stack, including its thick uppermost unit in the core of the Malolotsha Syncline, rests on a major thrust fault and forms a complex tectonic klippe; (c) Forward-modeled retrodeformed cross section of balanced section shown in panel b. Evolution is modeled as a forward-migrating thrust stack, in line with field observations and the cross section. After shortening of >33 km, the thrust stack was folded.

6.4. Tectonic Reconstruction

Unfolding the deformed stratigraphy along the line of cross-section and forward-modeling its thrust stack geometry in a balanced-cross-sectioning approach is a first step toward more detailed investigations and is subject to a number of assumptions and uncertainties:

1. The approach heavily depends on projected geology at depth (Figure 13a). It is based on projecting geological information into the line of cross section and using the geology of the hinge area to infer the geometry of synclinal fold closure at depth.
2. Kinematic forward modeling of the unfolded cross section is area- and line-length balanced, assuming the standard assumption of balanced cross-sectioning: Thicknesses remain constant, and there is no movement in or out the plane of section.
3. Neither fault-related folding nor (re-)activation of thrusts are involved in the folding of the thrust stack. Rather, the applied Flexural Slip algorithm rotates fold limbs to an orientation pre-defined by the cross-section template. It maintains both the area of the modeled unit and the line length along the template horizon but will preserve line lengths of other horizons only where they are oriented parallel to the template orientation. In the moderately-to-tightly folded Malolotsha region, this is rarely the case. Our approach thus yielded not a line-length- but an area-balanced cross-section.
4. No cut-off angles are preserved within the Onverwacht Group (Figure 13c); the modeled displacement is thus a minimum.
5. Modeling does not incorporate any ductile deformation which, as the conglomerate clast strain study suggests, may be significant, and may have been particularly high in the incompetent Onverwacht talc schists, as discussed in the previous chapter.
6. Lastly, the internal stratigraphy of the allochthonous sequence of the Onverwacht Group metavolcanics and cherts is largely destroyed by small-scale tight to isoclinal folding and by offsets along numerous poorly documented and largely unexposed faults and shear zones (Figures 2 and 4). This structural and stratigraphic complexity may be due to preexisting structures within the thrust sheet package, due to the significant competence contrast between the two stratigraphic packages, due to space problems developing during thrusting and folding, and locally by high ductile strain due to proximity of the study area to the high-strain southern margin of the BGB. Detailed geologic mapping at optimal outcrop conditions may be able to provide some clarity on this topic.

The minimum shortening inferred from our kinematic forward model is ca. 33 km, favorably comparing to Lamb's (1984, 1986) and Lamb and Paris's (1988) estimated displacement of "greater than 10 km." Each of the factors listed above, however, when quantified, would result in a higher degree of deformation and/or a higher displacement.

6.5. Direction of Tectonic Transport; Structural Style and Tectonic Architecture

The inferred transport direction from the balanced-cross-section modeling shows a displacement toward the NW, as proposed in early geological cross sections by Davies (1959), Pretorius (1961), and Jones (1963), and as discussed by Lamb (1984, 1987) and Lamb and Paris (1988). The increase in thrust sheet thickness from northwest (the leading-edge stack, a few hundred m at most) to the southeast (in the structurally highest levels, the core of the Malolotsha Syncline, a minimum of ca. 1,450 m) requires a significantly deeper initial detachment level to the southeast, stepping up toward the northwest along a series of ramps and flats (Figure 13c); this geometry is consistent with critical-taper geometry and an overall northwestward transport. The NW-SE trend of stretching lineations, approximately perpendicular to the regional dominant fold trend (F4 of Lowe et al., 1999, and of Lana, Tohver, & Cawood, 2010) and to the SE margin of the BGB, and the juxtaposition of older (Onverwacht Group) over younger (Moodies Group) strata is also consistent with the top-to-the-NW transport. Lamb and Paris (1988) assigned this displacement to a "late synsedimentary stage" of shortening (their D2b), related to coeval deformation and metamorphism in the AGC of southern Eswatini (Jackson, 1984) and named the subsequent deformation of the thrust sheet package into a synform "D3" (Lamb, 1984). Lamb and Paris (1988) estimated that both deformation phases shortened the Moodies basin by about 50% but provided no estimate of its original width. Both phases may be part of a single progressive deformation but because the orientations of shortening by folding and by imbrication appear parallel and because additional features (such as cross-cutting dike generations) have not been observed, no statement can be made. Lamb's (1984) mapping of intraformational progressive

unconformities in Moodies Group strata a few km to the southwest suggests that sedimentation and shortening (by folding or thrusting) overlapped each other. Updated terminology of BGB deformation phases (e.g., Byerly et al., 2019; Lana, Tohver, & Cawood, 2010; Schmitz & Heubeck, 2021) assign the Moodies-basin-forming extensional event to the D3 deformation phase, subsequent shortening and folding to D4a and D4b, respectively, and orogen-wide tightening, rotation into the vertical or beyond, and strike-slip faulting to D5. A similar sequence of events is inferred for constrictively strained Moodies Group conglomerates of the Ntaba Mhlope Syncline, located ca. 22 km along strike to the northeast.

To the knowledge of the authors, no tectonic style incorporating a similarly significant amount of subhorizontal shortening in Moodies strata is conclusively documented elsewhere in the BGB (see, e.g., the discussion of Van Kranendonk, 2021, of the “recumbent nappe pile” of de Wit, 1982, in the central BGB). The radiometric age data, strain analysis and cross-section balancing presented here strengthen, expand, and quantify the interpretations of Tankard et al. (1982), Jackson (1987), Lamb (1984, 1986), and Lamb and Paris (1988). These authors interpreted the folded thrust stack and the western limb of the Malolotsha Syncline as an “intermediate tectonic element” of a largely eroded, northwest-facing fold-and-thrust belt which likely extended along the entire length of the southeastern margin of the BGB. This belt was overridden in post-Moodies times by high-grade metamorphic and igneous units of the AGC to the southeast, now largely obscured by voluminous undeformed granite sheets of the Piggs Peak and Mpuluzi Batholiths (Anhaeusser & Robb, 1983; Hunter, 1970; Kröner & Tegtmeier, 1994; Moyen et al., 2021; Westraat et al., 2005). Only two small regions of the AGC are preserved adjacent to the BGB, both exposing high-grade gneisses and amphibolites: The Piggs Peak Inlier (Kröner et al., 1989, 1991, 2016; Figure 1) which is separated from the BGB by the complex, poorly exposed Phophonyane Shear Zone (Schoene et al., 2008); and the small, a few hundred m wide Malolotja Inlier (Lana et al., 2011; Schoene & Bowring, 2010) adjacent to the study area.

Approximately SE-NW directed major transport and shortening during Moodies time, as documented here by the orientation of the stretched conglomerate clasts, appears to be contemporaneous but is oriented perpendicular to the NE-SW trending stretching lineations at deeper structural levels, along the TTG-greenstone contacts, and in the marginal zones of many TTGs in the south (Kisters et al., 2003; Diener et al., 2005; Schoene et al., 2008; Lana, Kisters, & Stevens, 2010; Lana, Tohver, & Cawood, 2010; 2011). Numerous authors have compared this pattern to processes in modern orogens which show shortening (folding, thrusting, upright foliations) at upper structural levels while recording high-angle, orthogonal extrusion (collapse, channel flow) at lower structural levels (Grenville, Himalayas, Alps etc.; e.g., Jamieson et al., 2002; Beaumont et al., 2004; Jamieson & Beaumont, 2011; Scharf et al., 2013; Kelly et al., 2020). Because of the significantly different states of investigation along the northern (Badplaas–Barberton–Malelane), southwestern (Badplaas–Tjakastad - Steynsdorp) and southeastern (Oshoek–Malolotja–Piggs Peak–Hhohho) BGB margins, a regional comparison of their tectonic histories is problematic and also beyond the scope of this manuscript. A complex fold-and-thrust belt, first documented in the Malolotja and along the southeastern BGB margin by Lamb (1984), may also have formed in late Moodies and early post-Moodies time (ca. 3.22–3.21 Ga) along the northern margin (Byerly et al., 2019; Dziggel et al., 2006, 2010; Heubeck & Lowe, 1994; Otto et al., 2007; Zeh et al., 2009). Both belts may be contemporaneous with orogen-parallel extension, best documented along the southwestern margin (Diener et al., 2005; Kisters et al., 2003, 2010). However, the difference in Moodies conglomerate clast strain type, namely mainly plain strain (Anhaeusser, 1969; Ramsay, 1963) in the north and mainly constrictive strain in the southeast (Schmitz & Heubeck, 2021; this manuscript) may indicate a significant degree of asymmetry in syn- and post-Moodies D4 and D5 orogenic architecture.

The geology of the Malolotsha region appears to strengthen the relevance of a BGB deformation style and deformation phase which shows significant horizontal shortening relative to its vertical displacement. The relative contributions of either mode to Archean tectonics in general and to BGB geology in particular has long been a controversially discussed issue, and this contribution will not attempt to discuss it in detail; the reader is referred to recent regional (Drabon & Lowe, 2021; Schmitz & Heubeck, 2021) and review literature (Bédard, 2018; Byerly et al., 2019; de Wit et al., 2018; van Kranendonk, 2011a, 2011b etc.). Although there is wide agreement that the spatial and temporal interactions of vertical and horizontally-dominated tectonics in the BGB are as yet not fully understood, solid field-derived evidence for both modes appears to exist in the >340 Ma long rock record of the BGB and its numerous deformation phases.

7. Conclusions

The Malolotsha region near the southern margin of the BGB in Eswatini represents the largest and best-preserved tectonic structure to represent the dominant late-stage deformation style of the BGB at ca. 3.22 Ga. Northwestward-directed thrusting followed by tight folding resulted in a tightly folded imbricate stack of Onverwacht Group and Moodies Group strata which probably formed part of a much larger, northwestward-verging fold-and-thrust-belt-style orogen that extended along the entire southern margin of the BGB (Lamb, 1984; Lamb & Paris, 1988). U-Pb zircon dating of thin silicified felsic volcanics interbedded with a complex, >1 km thick sequence of altered ultramafic rocks shows that the structurally highest element in the Malolotsha thrust stack, the Malolotsha Syncline, places thick strata of the middle Onverwacht Group (ca. 3.34–3.31 Ga; Kromberg and Mendon formations) on Moodies Group (ca. 3.21 Ga) strata and forms a complex tectonic klippe. Orogenic structures and rocks adjacent to the BGB are largely obliterated or covered by large undeformed granitic sheets, hindering efforts to better constrain the dynamics and kinematics of this regional post-3.22 Ga shortening. Tectonic transport, inferred from strain analysis of conglomerate clasts in the study area and along the southern BGB margin, was to the northwest, that is, perpendicular to the present-day faulted, ductily strained and multiply metamorphosed southern margin of the BGB. Because these clasts show a significantly higher degree of prolate (constrictional) strain and because penetrative ductile strain extends far further into the BGB than recorded at its northern margin, late-stage BGB tectonic architecture may be distinctly asymmetrical.

Conflict of Interest

The authors declare no conflicts of interest relevant to this study.

Data Availability Statement

Analytical data for U-Pb age dating and strain data (Tables S1 and S2, respectively) are available at GFZ Data Services at <https://doi.org/10.5880/figeo.2022.037>. Both tables also include location information. The data are cited in Heubeck, Thomsen, et al. (2022).

References

- Anhaeusser, C. R. (1969). A comparison of pebble and fold deformation in the Nelspruit granite contact aureole, Barberton Mountain Land. *Transactions of the Geological Society of South Africa*, 72, 49–60.
- Anhaeusser, C. R. (1984). Structural elements of Archaean granite-greenstone terranes as exemplified by the Barberton Mountain Land, southern Africa. In A. Kröner & R. Greiling (Eds.), *Precambrian tectonics illustrated* (pp. 57–78). E. Schweizerbart'sche Verlagsbuchhandlung.
- Anhaeusser, C. R., & Robb, L. J. (1983). Geological and geochemical characteristics of the Heerenveen and Mpuluzi batholiths south of the Barberton greenstone belt and preliminary thoughts on their petrogenesis. *Geological Society of South Africa Special Publication*, 9, 131–151.
- Anhaeusser, C. R., Robb, L. J., & Viljoen, M. J. (1983). Notes on the provisional geological map of the Barberton greenstone belt and surrounding granitic terrane, Eastern Transvaal and Swaziland (1:250,000 colour map). *Special Publication - Geological Society of South Africa*, 9, 221–223.
- Anhaeusser, C. R., Roering, C., Viljoen, M. J., & Viljoen, R. P. (1968). The Barberton Mountain Land; a model of the elements and evolution of an Archaean fold belt. *Geological Society South Africa (annex)*, 71, 225–254.
- Barton, J. M. (1982). Geology and mineral resources of northwest Swaziland (Barberton greenstone belt). *Bulletin of the Geological Survey and Mines Department of Swaziland*, 10, 97.
- Beaumont, C., Jamieson, R. A., Nguyen, M. H., & Medvedev, S. (2004). Crustal channel flows: 1. Numerical models with applications to the tectonics of the Himalayan-Tibetan orogen. *Journal of Geophysical Research*, 109(B6), B06406. <https://doi.org/10.1029/2003JB002809>
- Bédard, J. H. (2006). A catalytic delamination-driven model for coupled Genesis of Archaean crust and subcontinental lithospheric mantle. *Geochimica et Cosmochimica Acta*, 70(5), 1188–1214. <https://doi.org/10.1016/j.gca.2005.11.008>
- Bédard, J. H. (2018). Stagnant lids and mantle overturns: Implications for Archaean tectonics, magmagenesis, crustal growth, mantle evolution, and the start of plate tectonics. *Geoscience Frontiers*, 9(1), 19–49. <https://doi.org/10.1016/j.gsf.2017.01.005>
- Black, L. P., Kamo, S. L., Allen, C. M., Davis, D. W., Aleinikoff, J. N., Valley, J. W., et al. (2004). Improved ²⁰⁶Pb/²³⁸U microprobe geochronology by the monitoring of a trace-element-related matrix effect; SHRIMP, ID-TIMS, ELA-ICP-MS and oxygen isotope documentation for a series of zircon standards. *Chemical Geology*, 205(1–2), 115–140. <https://doi.org/10.1016/j.chemgeo.2004.01.003>
- Bucher, K., & Frey, M. (1994). *Petrogenesis of metamorphic rocks* (6th ed., p. 318). Springer.
- Byerly, G. R. (1999). Komatiites of the Mendon Formation: Late-stage ultramafic volcanism in the Barberton greenstone belt. In D. R. Lowe & G. R. Byerly (Eds.), *Geologic evolution of the Barberton greenstone belt, South Africa*, *Geological Society of America* (Vol. 329, pp. 189–211).
- Byerly, G. R., Kröner, A., Lowe, D. R., Todt, W., & Walsh, M. M. (1996). Prolonged magmatism and time constraints for sediment deposition in the early Archaean Barberton greenstone belt: Evidence from the upper Onverwacht and fig tree groups. *Precambrian Research*, 78(1–3), 125–138. [https://doi.org/10.1016/0301-9268\(95\)00073-9](https://doi.org/10.1016/0301-9268(95)00073-9)
- Byerly, G. R., Lowe, D. R., & Heubeck, C. (2019). Geologic evolution of the Barberton greenstone belt – A unique record of crustal development, surface processes, & early life 3.55 to 3.20 Ga. In M. J. van Kranendonk, V. C. Bennett, & J. E. Hoffmann (Eds.), *Earth's oldest rocks* – (2nd ed., pp. 569–613). Elsevier.

Acknowledgments

Field work in Eswatini was supported by funds from Friedrich-Schiller-University Jena. Frank Linde and Sandra Urban are thanked for rock processing and thin-section preparation, respectively. Wisdom Mdimisani Dlamini and Sandile Gumede from the Eswatini National Trust Commission graciously permitted geological field work and sampling in the Malolotsha Reserve. Reserve Managers Ngwane Dlamini and Cornelius Mashaba, Science Officer Mandla Makhanya and his staff of the Malolotsha Reserve are thanked for hospitality and company in the field. Graduate students Paul Fugmann, Sami Nabhan, Martin Homann, Deon Janse van Rensburg, Sebastian Reimann, Matthias Schmitz, and Christoph Stoltenberg served as field assistants 2012–2021. Open Access funding enabled and organized by Projekt DEAL.

- Byerly, G. R., & Palmer, M. R. (1991). Tourmaline mineralization in the Barberton greenstone belt, South Africa: Early Archean metasomatism by evaporite-derived boron. *Contributions to Mineralogy and Petrology*, 107(3), 387–402. <https://doi.org/10.1007/bf00325106>
- Cawood, P. A., Kröner, A., & Pisarevsky, S. (2006). Precambrian plate tectonics: Criteria and evidence. *Geological Society of America*, 16, 4–11.
- Cloete, M. (1999). Aspects of volcanism and metamorphism of the Onverwacht Group lavas in the southwestern portion of the Barberton greenstone belt. *Geological Society of South Africa, Memoir*, 84, 232.
- Condie, K. C., & Kröner, A. (2008). When did plate tectonics begin? Evidence from the geological record. *Geological Society of America Special Paper*, 440, 281–295.
- Cutts, K. A., Stevens, G., Hoffmann, J. E., Buick, I. S., Frei, D., & Münker, C. (2014). Paleo-to Mesoarchean polymetamorphism in the Barberton granite-greenstone belt, South Africa: Constraints from U-Pb monazite and Lu-Hf garnet geochronology on the tectonic processes that shaped the belt. *The Geological Society of America Bulletin*, 126(3–4), 251–270. <https://doi.org/10.1130/b30807.1>
- Davies, D. N. (1959). The intrusion of the Jamestown igneous complex in Swaziland. In *XXth International Geological Congress* (pp. 69–74).
- Decker, N. B., Byerly, G. R., Stüegler, M., Lowe, D. R., & Stefurak, E. (2015). High resolution tephra and U/Pb chronology of the 3.33-3.26 Ga Mendon Formation, Barberton greenstone belt, South Africa. *Precambrian Research*, 261, 54–74. <https://doi.org/10.1016/j.precamres.2015.02.003>
- de Ronde, C. E. J., & de Wit, M. J. (1994). Tectonic history of the Barberton greenstone belt, South Africa: 490 million years of Archean evolution. *Tectonics*, 13(4), 983–1005. <https://doi.org/10.1029/94tc00353>
- de Wit, M. J. (1982). Gliding and overthrust nappe tectonics in the Barberton greenstone belt. *Journal of Structural Geology*, 4(2), 117–136. [https://doi.org/10.1016/0191-8141\(82\)90022-0](https://doi.org/10.1016/0191-8141(82)90022-0)
- de Wit, M. J. (1991). Archean greenstone belt tectonism and basin development: Some insights from the Barberton and Pietersburg greenstone belts, Kaapvaal Craton, South Africa. *Journal of African Earth Sciences*, 13(1), 45–63. [https://doi.org/10.1016/0899-5362\(91\)90043-x](https://doi.org/10.1016/0899-5362(91)90043-x)
- de Wit, M. J., Fripp, R. E. P., & Stanistreet, I. G. (1983). Tectonic and stratigraphic implications of new field observations along the southern part of the Barberton Greenstone Belt. *Geological Society of South Africa Special Publication*, 9, 21–29.
- de Wit, M. J., Furnes, H., MacLennan, S., Doucouré, M., Schoene, B., Weckmann, U., et al. (2018). Paleoproterozoic bedrock lithologies across the Makhonjwa Mountains of South Africa and Swaziland linked to geochemical, magnetic and tectonic data reveal early plate tectonic genes flanking subduction margins. *Geoscience Frontiers*, 9(3), 603–665. <https://doi.org/10.1016/j.gsf.2017.10.005>
- de Wit, M. J., Roering, C., Hart, R. J., Armstrong, R. A., de Ronde, C. E. J., Green, R. W. E., et al. (1992). formation of an Archean continent. *Nature*, 357(6379), 553–562. <https://doi.org/10.1038/357553a0>
- Diener, J. F. A., Stevens, G., Kisters, A., & Poujol, M. (2005). Metamorphism and exhumation of the basal parts of the Barberton greenstone belt, South Africa: Constraining the rates of Mesoarchean tectonism. *Precambrian Research*, 143(1–4), 87–112. <https://doi.org/10.1016/j.precamres.2005.10.001>
- Diener, J. G., Stevens, G., & Kisters, A. F. M. (2006). High-pressure, low-temperature metamorphism in the southern Barberton granitoid greenstone terrain, South Africa: A record of overthickening and collapse of mid-Archean continental crust. In K. Benn, J.-C. Mareschal, & K. C. Condie (Eds.), *Archean geodynamic processes* (Vol. 164, pp. 239–254). American Geophysical Union Monograph.
- Drabon, N., & Lowe, D. R. (2021). Progressive accretion recorded in sedimentary rocks of the 3.28–3.23 Ga fig tree group, Barberton greenstone belt. *The Geological Society of America Bulletin*, 19(5–6), 1258–1276. <https://doi.org/10.1130/B35973.1>
- Dziggel, A., Armstrong, R. A., Stevens, G., & Nasdala, L. (2005). Growth of zircon and titanite during metamorphism in the granitoid-greenstone terrain south of the Barberton greenstone belt, South Africa. *Mineralogical Magazine*, 69, 1021–1038.
- Dziggel, A., Knipfer, S., Kisters, A. F. M., & Meyer, F. M. (2006). P-T and structural evolution during exhumation of high-T, medium-P basement rocks in the Barberton Mountain Land. *Journal of Metamorphic Geology*, 24(7), 535–551. <https://doi.org/10.1111/j.1525-1314.2006.00653.x>
- Dziggel, A., Poujol, M., Otto, A., Kisters, A. F. M., Trieloff, M., Schwarz, W. H., & Meyer, F. M. (2010). New U–Pb and ⁴⁰Ar/³⁹Ar ages from the northern margin of the Barberton greenstone belt, South Africa: Implications for the formation of Mesoarchean gold deposits. *Precambrian Research*, 179(1–4), 206–220. <https://doi.org/10.1016/j.precamres.2010.03.006>
- Egan, S. S., Buddin, T. S., Kane, S., & Williams, G. D. (1997). Three-dimensional modelling and visualisation in structural geology: New techniques for the restoration and balancing of volumes. In *Proceedings of the 1996 geoscience information group conference on geological visualisation*. In *Electronic geology special* (Vol. 1, pp. 67–82).
- Ganguly, J. (1969). Chloritoid stability and related parageneses: Theory, experiments, and applications. *American Journal of Science*, 267(8), 910–944. <https://doi.org/10.2475/ajs.267.8.910>
- Geological Survey of Swaziland. (1970). *Sheet 3 Forbes Reef. 1:25,000 series geological maps*. Swaziland Geological Survey and Mines Department.
- Gerdes, A., & Zeh, A. (2006). Combined U–Pb and Hf isotope LA-(MC)-ICP-MS analyses of detrital zircons: Comparison with SHRIMP and new constraints for the provenance and age of an Armorican metasediment in Central Germany. *Earth and Planetary Science Letters*, 249(1–2), 47–61. <https://doi.org/10.1016/j.epsl.2006.06.039>
- Gerdes, A., & Zeh, A. (2009). Zircon formation versus zircon alteration – New insights from combined U–Pb and Lu–Hf in-situ LA-ICP-MS analyses, & consequences for the interpretation of Archean zircon from the Central Zone of the Limpopo Belt. *Chemical Geology*, 261(3–4), 230–243. <https://doi.org/10.1016/j.chemgeo.2008.03.005>
- Hellstrom, J., Paton, C., Woodhead, J., & Hergt, J. (2008). Iolite: Software for spatially resolved LA- (quad and MC) ICPMS analysis. In P. Sylvester (Ed.), *Laser ablation ICP-MS in the earth sciences: Current practices and outstanding issues*, 343–348. Mineral. Assoc. of Canada.
- Heubeck, C. (2019). The Moodies Group - a high-resolution archive of Archean surface and basin-forming processes. In A. Kröner & A. Hofmann (Eds.), *The Archean geology of the Kaapvaal Craton, Southern Africa* (pp. 203–241). Springer (Regional Geology Reviews). https://doi.org/10.1007/978-3-319-78652-0_6
- Heubeck, C., Drabon, N., Byerly, G., Leisgang, I., Linnemann, U., Lowe, D. R., et al. (2022). Constraints by detrital zircons on the provenance of the Archean Moodies group, Barberton greenstone belt, South Africa and Eswatini. *American Journal of Science*, 322, 65–107.
- Heubeck, C., Engelhardt, J., Byerly, G. R., Zeh, A., Sell, B., Lubert, T., & Lowe, D. R. (2013). Timing of deposition and deformation of the Moodies group (Barberton greenstone belt, South Africa): Very-high-resolution of Archean surface processes. *Precambrian Research*, 231, 236–262. <https://doi.org/10.1016/j.precamres.2013.03.021>
- Heubeck, C., & Lowe, D. R. (1994). Late syndepositional deformation and detachment tectonics in the Barberton greenstone belt, South Africa. *Tectonics*, 13(6), 1514–1536. <https://doi.org/10.1029/94tc01809>
- Heubeck, C., & Lowe, D. R. (1999). Sedimentary petrology and provenance of the Archean Moodies group, Barberton greenstone belt, South Africa. In D. R. Lowe & G. R. Byerly (Eds.), *Geologic evolution of the Barberton greenstone belt, South Africa, Geological society of America* (Vol. 329, pp. 259–286).

- Heubeck, C., Thomsen, T. B., Heredia, B. D., Zeh, A., & Balling, P. (2022). U-Pb data from cherts (Onverwacht group) and strain data from conglomerates (Moodies group) from the southern margin of the Archean Barberton greenstone belt. *Eswatini. GFZ Data Services*. <https://doi.org/10.5880/figeo.2022.037>
- Hiess, J., Condon, D. J., McLean, N., & Noble, S. R. (2012). 238U/235U systematics in terrestrial uranium-bearing minerals. *Science*, 335(6076), 1610–1614. <https://doi.org/10.1126/science.1215507>
- Hunter, D. R. (1970). The ancient Gneiss complex in Swaziland. *South African Journal of Geology*, 73, 107–150.
- Jackson, M. P. A. (1984). Archean structural styles in the ancient Gneiss complex of Swaziland, southern Africa. In A. Kröner (Ed.), *Precambrian tectonics illustrated*. E. Schweizerbart'sche Verlagsbuchhandlung.
- Jackson, M. P. A., & Robertson, D. I. (1983). Regional implications of early-Precambrian strains in the Onverwacht group adjacent to the Lochiel granite, north-west Swaziland. *Geological Society of South Africa Special Publication*, 9, 45–62.
- Jackson, S. E., Pearson, N. J., Griffin, W. L., & Belousova, E. A. (2004). The application of laser ablation-inductively coupled plasma-mass spectrometry to in situ U–Pb zircon geochronology. *Chemical Geology*, 211(1–2), 47–69. <https://doi.org/10.1016/j.chemgeo.2004.06.017>
- Jamieson, R. A., & Beaumont, C. (2011). Coeval thrusting and extension during lower crustal ductile flow - Implications for exhumation of high-grade metamorphic rocks. *Journal of Metamorphic Geology*, 29(1), 33–51. <https://doi.org/10.1111/j.1525-1314.2010.00908.x>
- Jamieson, R. A., Beaumont, C., Nguyen, M. H., & Lee, B. (2002). Interaction of metamorphism, deformation and exhumation in large convergent orogens. *Journal of Metamorphic Geology*, 20(1), 9–24. <https://doi.org/10.1046/j.0263-4929.2001.00357.x>
- Jones, D. H. (1963). Geology of the Malolotsha Valley. *Bulletin of the Geological Survey and Mines Department*, 3, 17–27.
- Kelly, S., Beaumont, C., & Butler, J. P. (2020). Inherited terrane properties explain enigmatic post-collisional Himalayan-Tibetan evolution. *Geology*, 48(1), 8–14. <https://doi.org/10.1130/G46701.1>
- Kisters, A. F. M., Belcher, R. W., Pujol, M., & Dziggel, A. (2010). Continental growth and convergence-related arc plutonism in the Mesoarchean: Evidence from the Barberton granitoid-greenstone terrain, South Africa. *Precambrian Research*, 178(1–4), 15–26. <https://doi.org/10.1016/j.precamres.2010.01.002>
- Kisters, A. F. M., Stevens, G., Dziggel, A., & Armstrong, R. A. (2003). Extensional detachment faulting and core-complex formation in the southern Barberton granite-greenstone terrain, South Africa: Evidence for a 3.2 Ga orogenic collapse. *Precambrian Research*, 127(4), 355–378. <https://doi.org/10.1016/j.precamres.2003.08.002>
- Kröner, A., Anhaeusser, C. R., Hoffmann, J. E., Wong, J., Geng, H., Hegner, E., et al. (2016). Chronology of the oldest supracrustal sequences in the Palaeoarchean Barberton greenstone belt, South Africa and Swaziland. *Precambrian Research*, 279, 123–143. <https://doi.org/10.1016/j.precamres.2016.04.007>
- Kröner, A., Byerly, G. R., & Lowe, D. R. (1991). Chronology of early Archean granite-greenstone evolution in the Barberton Mountain Land, South Africa, based on precise dating by single zircon evaporation. *Earth and Planetary Science Letters*, 103(1–4), 41–54. [https://doi.org/10.1016/0012-821x\(91\)90148-b](https://doi.org/10.1016/0012-821x(91)90148-b)
- Kröner, A., Compston, W., & Williams, I. S. (1989). Growth of early Archean crust in the Ancient Gneiss Complex of Swaziland as revealed by single zircon dating. *Tectonophysics*, 161(3–4), 271–298. [https://doi.org/10.1016/0040-1951\(89\)90159-5](https://doi.org/10.1016/0040-1951(89)90159-5)
- Kröner, A., Hegner, E., Wendt, J. I., & Byerly, G. R. (1996). The oldest part of the Barberton granitoid-greenstone terrain, South Africa: Evidence for crust formation between 3.5 and 3.7 Ga. *Precambrian Research*, 78(1–3), 105–124. [https://doi.org/10.1016/0301-9268\(95\)00072-0](https://doi.org/10.1016/0301-9268(95)00072-0)
- Kröner, A., & Hofmann, A. (Eds.) (2019). *The Archean geology of the Kaapvaal Craton, Southern Africa* (p. 302). Springer.
- Kröner, A., & Tegtmeier, A. (1994). Gneiss-greenstone relationships in the Ancient Gneiss Complex of southwestern Swaziland, southern Africa, & implications for early crustal evolution. *Precambrian Research*, 67(1–2), 109–139. [https://doi.org/10.1016/0301-9268\(94\)90007-8](https://doi.org/10.1016/0301-9268(94)90007-8)
- Kröner, A., Wong, J., & Xie, H. (2018). The oldest granite clast in the Moodies conglomerate, Barberton Greenstone Belt, South Africa, and its likely origin. *South African Journal of Geology*, 121(1), 43–50. <https://doi.org/10.25131/sajg.121.0001>
- Lamb, S. H. (1984). Structures on the eastern margin of the Archean Barberton greenstone belt. In A. Kröner (Ed.), *Precambrian tectonics illustrated*. E. Schweizerbart'sche Verlagsbuchhandlung.
- Lamb, S. H. (1986). *Synsedimentary deformation and thrusting on the eastern margin of the Barberton Greenstone Belt, Swaziland* (pp. N86–25910). Lunar and Planetary Conference.
- Lamb, S. H. (1987). Archean synsedimentary tectonic deformation – a comparison with the Quaternary. *Geology*, 15(6), 565–568. [https://doi.org/10.1130/0091-7613\(1987\)15<565:astdcw>2.0.co;2](https://doi.org/10.1130/0091-7613(1987)15<565:astdcw>2.0.co;2)
- Lamb, S. H., & Paris, I. (1988). Post-Onverwacht stratigraphy in the southeastern part of the Archean Barberton greenstone belt. *Journal of African Earth Sciences*, 7(1), 285–306. [https://doi.org/10.1016/0899-5362\(88\)90074-7](https://doi.org/10.1016/0899-5362(88)90074-7)
- Lana, C., Buick, I., Stevens, G., Roussow, R., & de Wet, W. (2011). 3230–3200 Ma post-orogenic extension and mid-crustal magmatism along the southeastern margin of the Barberton Greenstone Belt, South Africa. *Journal of Structural Geology*, 33(5), 844–858. <https://doi.org/10.1016/j.jsg.2011.03.007>
- Lana, C., Kisters, A., & Stevens, G. (2010). Exhumation of Mesoarchean TTG gneisses from the middle crust: Insights from the Steynsdorp core complex, Barberton granitoid-green stone terrain, South Africa. *The Geological Society of America Bulletin*, 122(1–2), 183–197. <https://doi.org/10.1130/b26580.1>
- Lana, C., Tohver, E., & Cawood, P. (2010). Quantifying rates of dome-and-keel formation in the Barberton granitoid-greenstone belt, South Africa. *Precambrian Research*, 177(1–2), 199–211. <https://doi.org/10.1016/j.precamres.2009.12.001>
- Lowe, D. R. (1999). Geologic evolution of the Barberton greenstone belt and vicinity. In D. R. Lowe & G. R. Byerly (Eds.), *Geologic evolution of the Barberton greenstone belt, South Africa* (Vol. 329, pp. 287–312). Geological Society of America, Special Paper.
- Lowe, D. R., & Byerly, G. R. (1999). Stratigraphy of the west-central part of the Barberton greenstone belt, South Africa. *Geological Society of America, Special Paper*, 329, 1–36.
- Lowe, D. R., & Byerly, G. R. (2007). An overview of the geology of the Barberton Greenstone Belt and vicinity: Implications for early crustal development. In M. J. van Kranendonk, R. H. Smithies, & V. H. Bennett (Eds.), *Earth's oldest rocks* (Vol. 15, pp. 481–526). Elsevier (Developments in Precambrian Geology).
- Lowe, D. R., Byerly, G. R., & Heubeck, C. (1999). Structural divisions and development of the west-central part of the Barberton Greenstone Belt. In D. R. Lowe & G. R. Byerly (Eds.), *Geologic evolution of the Barberton greenstone belt, South Africa* (Vol. 329, pp. 37–82). Geological Society of America, Special Paper.
- Moyen, J.-F., Stevens, G., Kisters, A. F. M., & Belcher, B. L. (2018). TTG plutons of the Barberton granitoid-greenstone terrain, South Africa. In M. J. van Kranendonk, V. C. Bennett, & J. E. Hoffmann (Eds.), *Earth's oldest rocks – (2nd ed., pp. 607–667)*. Elsevier.
- Moyen, J.-F., Zeh, A., Cuney, M., Dziggel, A., & Carroué, S. (2021). The multiple ways of recycling Archean crust: A case study from the ca. 3.1 Ga “late” granitoids from the Barberton greenstone belt, South Africa. *Precambrian Research*, 353, 105998. <https://doi.org/10.1016/j.precamres.2020.105998>

- Otto, A., Dziggel, A., Kisters, A. F. M., & Meyer, F. M. (2007). The new consort gold mine, Barberton greenstone belt, South Africa: Orogenic gold mineralization in a condensed metamorphic profile. *Mineralium Deposita*, 42(7), 715–735. <https://doi.org/10.1007/s00126-007-0135-5>
- Palin, R. M., Santosh, M., Cao, W., Li, S.-S., Hernández-Urbe, D., & Parsons, A. (2020). Secular change and the onset of plate tectonics on Earth. *Earth-Science Reviews*, 207, 103172. <https://doi.org/10.1016/j.earscirev.2020.103172>
- Paton, C., Hellstrom, J. C., Paul, P., Woodhead, J. D., & Hergt, J. M. (2011). Iolite: Freeware for the visualisation and processing of mass spectrometric data. *Journal of Analytical Atomic Spectrometry*, 26(12), 2508–2518. <https://doi.org/10.1039/c1ja10172b>
- Paton, C., Woodhead, J. D., Hellstrom, J. C., Hergt, J. M., Greig, A., & Maas, R. (2010). Improved laser ablation U-Pb zircon geochronology through robust downhole fractionation correction. *Geochemistry, Geophysics, Geosystems*, 11(3), 1–36. <https://doi.org/10.1029/2009gc002618>
- Petrus, J. A., & Kamber, B. S. (2012). VizualAge: A novel approach to laser ablation ICP-MS U-Pb geochronology data reduction. *Geostandards and Geoanalytical Research*, 36(3), 247–270. <https://doi.org/10.1111/j.1751-908x.2012.00158.x>
- Pretorius, D. A. (1961). *The geology of a portion of the country between the Komati and Usushwana Rivers* (Vol. 1, pp. 56–83). Swaziland Geological Survey and Mines Department.
- Ramsay, J. G. (1963). Structural investigations in the Barberton Mountain land, eastern Transvaal. *Transactions of the Geological Society of South Africa*, 66, 353–398.
- Reimann, S., Heubeck, C., Janse van Rensburg, D. J., Fugmann, P., Serre, S. H., Thomsen, T. B., & Zametzer, A. (2021). Syndepositional hydrothermalism selectively preserves records of one of the earliest benthic ecosystems, Moodies Group (3.22 Ga), Barberton Greenstone Belt, South Africa. *South African Journal of Geology*, 124(1), 253–278. <https://doi.org/10.25131/sajg.124.0012>
- Santos, M. M., Lana, C., Scholz, R., Buick, I., Schmitz, M. D., Kamo, S. L., et al. (2017). A new appraisal of Sri Lankan BB zircon as a reference material for LA-ICP-MS U-Pb geochronology and Lu-Hf isotope tracing. *Geostandards and Geoanalytical Research*, 41(3), 335–358. <https://doi.org/10.1111/ggr.12167>
- Scharf, A., Handy, M. R., Favaro, S., Schmid, S. M., & Bertrand, A. (2013). Modes of orogen-parallel stretching and extensional exhumation in response to microplate indentation and roll-back subduction (Tauern Window, Eastern Alps). *International Journal of Earth Sciences*, 102(6), 1627–1654. <https://doi.org/10.1007/s00531-013-0894-4>
- Schmitz, M., & Heubeck, C. (2021). Constraints on deformation mechanisms of the Barberton Greenstone Belt from regional stratigraphic and structural data of the synorogenic Moodies Group. *Precambrian Research*, 362, 106177. <https://doi.org/10.1016/j.precamres.2021.106177>
- Schoene, B., & Bowring, S. (2010). Rates and mechanisms of Mesoarchean magmatic arc construction, eastern Kaapvaal craton, Swaziland. *The Geological Society of America Bulletin*, 122(3–4), 408–429. <https://doi.org/10.1130/b26501.1>
- Schoene, B., de Wit, M. J., & Bowring, S. A. (2008). Mesoarchean assembly and stabilization of the eastern Kaapvaal craton: A structural-thermochronological perspective. *Tectonics*, 27(5), TC5010. <https://doi.org/10.1029/2008TC002267>
- Sláma, J., Košler, J., Condon, D. J., Crowley, J. L., Gerdes, A., Hanchar, J. M., et al. (2008). Plešovice zircon—A new natural reference material for U-Pb and Hf isotopic microanalysis. *Chemical Geology*, 249(1–2), 1–35. <https://doi.org/10.1016/j.chemgeo.2007.11.005>
- Stacey, J. S., & Kramers, J. D. (1975). Approximation of terrestrial lead isotope evolution by a two-stage model. *Earth and Planetary Science Letters*, 26(2), 207–221. [https://doi.org/10.1016/0012-821x\(75\)90088-6](https://doi.org/10.1016/0012-821x(75)90088-6)
- Tankard, A. J., Jackson, M. P. A., Eriksson, K. A., Hobday, D. K., Hunter, D. R., & Minter, W. E. L. (1982). Granite-greenstone terrane: Kaapvaal Province. In A. J. Tankard, M. P. A. Jackson, K. A. Eriksson, D. K. Hobday, D. R. Hunter, & W. E. L. Minter (Eds.), *Crustal evolution of Southern Africa* (pp. 21–86). Springer-Verlag Berlin.
- Tanner, P. W. G. (1989). The flexural-slip mechanism. *Journal of Structural Geology*, 11(6), 635–655. [https://doi.org/10.1016/0191-8141\(89\)90001-1](https://doi.org/10.1016/0191-8141(89)90001-1)
- Thompson Stiegler, M., Lowe, D. R., & Byerly, G. R. (2010). The petrogenesis of volcanoclastic Komatiites in the Barberton greenstone belt, South Africa: A textural and geochemical study. *Journal of Petrology*, 51(4), 947–972. <https://doi.org/10.1093/petrology/egq008>
- Tice, M. M., Bostick, B. C., & Lowe, D. R. (2004). Thermal history of the 3.5–3.2 Ga Onverwacht and Fig Tree Groups, Barberton greenstone belt, South Africa, inferred by Raman microspectroscopy of carbonaceous material. *Geology*, 32(1), 37–40. <https://doi.org/10.1130/g19915.1>
- Toulkeridis, T., Goldstein, S. L., Clauer, N., Kröner, A., Todt, W., & Schidlowski, M. (1998). Sm-Nd, Rb-Sr and Pb-Pb dating of silicic carbonates from the early Archaean Barberton Greenstone Belt, South Africa: Evidence for post-depositional isotopic resetting at low temperature. *Precambrian Research*, 92(2), 129–144. [https://doi.org/10.1016/s0301-9268\(98\)00071-0](https://doi.org/10.1016/s0301-9268(98)00071-0)
- Travers, L. (2020). *Caractérisation et distribution de l'évènement « or » dans la ceinture de roches vertes de Barberton (Afrique du Sud)* (p. 47). Unpublished MSc thesis, Rapport de stage.
- Urie, J. G. (1970). Sheet 3 – Forbes Reef (1:25 000 series map). *Swaziland Geol. Surv. Mines Dep.*
- Urie, J. G. (1971). Sheet 4 – Motjane (1:25 000 series map). *Swaziland Geol. Surv. Mines Dep.*
- Van Kranendonk, M. J. (2011a). Cool greenstone drips, hot rising domes, & the role of partial convective overturn in Barberton greenstone belt evolution. *Journal of African Earth Sciences*, 60(5), 346–352. <https://doi.org/10.1016/j.jafrearsci.2011.03.012>
- Van Kranendonk, M. J. (2011b). Onset of plate tectonics. *Science*, 333(6041), 413–414. <https://doi.org/10.1126/science.1208766>
- Van Kranendonk, M. J. (2021). Gliding and overthrust nappe tectonics of the Barberton greenstone belt revisited: A review of deformation styles and processes. *South African Journal of Geology*, 124(1), 181–210. <https://doi.org/10.25131/sajg.124.0017>
- Vermeesch, P. (2018). IsoplotR: A free and open toolbox for geochronology. *Geoscience Frontiers*, 9(5), 1479–1493. <https://doi.org/10.1016/j.gsf.2018.04.001>
- Vermeesch, P. (2021). On the treatment of discordant detrital zircon U-Pb data. *Geochronology*, 3(1), 247–257. <https://doi.org/10.5194/gchron-3-247-2021>
- Visser, D. J. L., van Eeden, O. R., Joubert, G. K., Söhne, A. P. G., van Zyl, J. S., Rossouw, J., et al. (1956). The geology of the Barberton area. *Geological Survey of South Africa Special Publication*, 15, 253.
- Westraat, J. D., Kisters, A. F. M., Poujol, M., & Stevens, G. (2005). Transcurrent shearing, granite sheeting and the incremental construction of the tabular 3.1 Ga Mpuluzi batholith, Barberton granite-greenstone terrane, South Africa. *Journal of the Geological Society of London*, 162(2), 373–388. <https://doi.org/10.1144/0016-764904-026>
- Wiechert, A. (2014). *Contributions to the geochronology of the northern and southern facies of the Archean Moodies group (Barberton greenstone belt, South Africa and Swaziland): M.Sc. Thesis* (p. 81). Freie Universität Berlin.
- Wiedenbeck, M., Allé, P., Corfu, F., Griffin, W. L., Meier, M., Oberli, F., et al. (1995). Three natural zircon standards for U-Th-Pb, Lu-Hf, trace element and REE analyses. *Geostandards Newsletter*, 19, 1–23. <https://doi.org/10.1111/j.1751-908x.1995.tb00147.x>
- Wiedenbeck, M., Hanchar, J. M., Peck, W. H., Sylvester, P., Valley, J., Whitehouse, M., et al. (2004). Further characterisation of the 91500 zircon crystal. *Geostandards and Geoanalytical Research*, 28(1), 9–39. <https://doi.org/10.1111/j.1751-908x.2004.tb01041.x>
- Xie, X., Byerly, G. R., & Ferrell, R. E. (1997). Ilb trioctahedral chlorite from the Barberton greenstone belt: Crystal structure and rock composition constraints with implications for geothermometry. *Contributions to Mineralogy and Petrology*, 126(3), 275–291. <https://doi.org/10.1007/s004100050250>

- Zeh, A., Gerdes, A., & Barton, J. M. (2009). Archean accretion and crustal evolution of the Kalahari Craton—the zircon age and Hf isotope record of granitic rocks from Barberton/Swaziland to the Francistown arc. *Journal of Petrology*, *50*(5), 933–966. <https://doi.org/10.1093/petrology/egp027>
- Zeh, A., Gerdes, A., & Heubeck, C. (2013). U-Pb and Hf isotope data of detrital zircons from the Barberton Greenstone Belt: Constraints on provenance and Archaean crustal evolution. *Journal of the Geological Society of London*, *170*(1), 215–223. <https://doi.org/10.1144/jgs2011-162>
- Zeh, A., Gerdes, A., & Millonig, L. (2011). Hafnium isotope record of the Ancient Gneiss Complex, Swaziland, southern Africa; evidence for Archaean crust–mantle formation and crust reworking between 3.66 and 2.73 Ga. *Journal of the Geological Society of London*, *168*(4), 1–11. <https://doi.org/10.1144/0016-76492010-117>